SILICON NANOSTRUCTURES

A Graduate Project Submitted to
The School of Graduate Studies of
Addis Ababa University

In partial Fulfillment of The
Requirements For The Degree of
Masters of Science in Physics

By

Tadesse Tenaw Kassa

Addis Ababa
Ethiopia

June 2006

ADDIS ABABA UNIVERSITY

SCHOOL OF GRADUATE STUDIES

SILICON NANOSTRUCTURES

BY
TADESSE TENAW KASSA

Department of Physics
Faculty of Science

Approved by the Examination Committee

Name	Signature
…Dr.S.K.Ghoshal……. …… Advisor	…….
Dr.Mulugeta Bekele…..…….. Examiner	……
…….. Examiner	…….

Contents **Page**

Acknowledgement

First and for most, I would like to acknowledge my advisor, Dr. S.K. Ghoshal, for his comments, suggestions and genuine advises he offered me during the progress of this work. His dedication, knowledge and skill as a qualified instructor and advisor are an inspiration. Thank you.

I am very grateful to my sweetheart, Kanchiwodia Wubshet. Her encouragements and patience to attend our kids was the engine of my career. Had it not been for her support, I, certainly, would not have succeeded.

I am deeply indebted to the AMHARA NATIONAL REGIONAL EDUCATION BUREAU for offering me the sponsorship to join the school of graduate studies.

Thank you Melaku and Sileshi! All what you have done for me is beyond words to descibe.

I wish also to thank Ato Desalegn Abebe, principal of D.M.H.E. preparatory school, along with the rest of the administrative staff, for his material support and other co-operations.

At last, but certainly not the least, I would like to acknowledge the technical and administrative staff of the Department of physics (A.A.U.). Their contribution was indeed indispensable.

Abstract

Low dimensional nano crystals are known to have properties that can be markedly different from their bulk counterparts .For semiconductor crystals such as silicon when the carriers (excitons) are confined in dimensions less than their de Broglie wavelength (typically a few nanometers) quantum mechanical size effects emerge.

In this dissertation the effects of these quantum confinements in silicon nanostructures are discussed in detail.

Moreover, the different synthesis methods of silicon nanostructures and the accompanying characterizations of silicon nanocrystals and porous silicon are illustrated briefly. Theoretical analysis of the electronic structures of silicon nanocrystals of small number of atoms using pseudo potential-DFT method is presented.

Finally the potential applications of these crystals in the electronic industry, nanobiotechnology and medicine are pointed out shortly.

Precisely the purpose of this dissertation is, thus, to review:

- What nanostructures are?
- What nanotechnology is?
- How quantum confinement affects a nanostructure?
- How silicon and its properties behave at nano scale?
- What methods are used to synthesize silicon nanostructures?
- How computational approximation methods are applied on nanostructures?
- What future outlooks regarding nanoscience and nanotechnology prevail?
- What potential applications does Silicon nanostructures in particular and Nanotechnologies in general have?

Introduction

Nanotechnology is essentially any application of science at or around the nanometer scale, and can be defined in simple terms as “engineering at a very small scale”. Silicon chip technology, the ability to manufacture at 100nm and below, and microscopes that allow us not only to see but also to manipulate atoms and molecules have plugged us at the start of the 21^{st} century in to the thick of science revolution.

Silicon is the leading material concerning high-density electronic functionality. Nanostructuring silicon is an effective way to turn silicon in to a photonic material. The small size results in new quantum phenomena that yield some extra ordinary bonuses. Material properties change drastically because quantum effects arise from the confinement of electrons and holes in the material.

At nano scale short rang forces such as van der Waal forces predominate. Gravity is less important.

Efficient emission of visible light has been observed from nanostructure of silicon. Although some controversial interpretation of the visible light emission from low-dimensional Si structures still exist, it is generally accepted that quantum confinement, caused by the restricted size, is essential for this phenomenon but actually not sufficient. Quantum confinment effect in the nanocrystallites opens up the energy band gap as well as relaxes the selection rules for radiative transmissions giving rise to photoluminescence in the visible range for crystallites size below ~5nm.

In this dissertation a short review of nonostructures and nanotechnology is given in the second and third chapters respectively. The concept of quantum confinement and its effects on density of state and energy gap of nanostructures is discussed in chapter four.

In chapter five short review of elemental silicon (bulk) is presented.

Porous silicon is a network of holes within an interconnected silicon matrix. The size of these air holes, called pores, can vary from a few nanometers to a few microns depending on the conditions of formation and the characteristics of silicon. The discussion in chapter six focuses on the formation, structure and properties of this material.

In chapter seven the subject of silicon nanocrystal, its formation, characterization and properties is treated in detail.

Pseudo-potential-DFT methods are implemented to investigate the structural and electrical properties of nanostructures. In chapter eight, this method is discussed shortly to apply it in analyzing nanostructures of silicon crystal.

Chapter nine previews the concepts of quasi-particle gap, HOMO-LUMO, and their inter relationships with optical gap energy.

Finally, potential applications and future out looks about silicon nanocrystals in particular and nanotechnology in general is discussed.

UNIT-ONE

Nanostructures

All the science of nanotechnology relies on nanoscale structures and the associated quantum confinement effects that lead them to spectacular features. The focus of this chapter is to investigate the nature of these structures and the subsequent effects a material faces due to miniaturization.

Structures of materials characterized by dimensions in the order of nanometer constitute nanostructures. Nanostructures are seen as the key for many applications in data storage, communications and biotechnology. A nanometer is incredibly small, about 50,000 times finer than a human hair and still 200 times smaller than the finest lithographic feature in microchips today. Yet, a cubic meter still contains quite a few atoms (something like 50 Si-atoms or 180 C-atoms) [1]. In this size regime, the law of quantum mechanics predominates.

The ultimate goal will be to operate devices with a single electron, atom by atom or molecule by molecule, but different atoms need to be separated from each other by a nanometer sized buffer. This way they stay independent of each other and do not form an ordinary chemical compound or alloy. .

Another characteristic of nanostructures is the dominant role played by surface and interface. Take for example a cube of 10 atoms on each side, which would be about 2-3 nm in size for a typical atom diameter of 0.2-0.3nm [1]. It contains comparable numbers of bulk and surface atoms. Nanostructures are so small that they may be viewed as an object consisting mainly of interfaces with no bulk behind them. In this case, the Hamiltonian differs from that of a bulk material. For example, the band gap at CaF_2 / Si (111) interface is more than twice as long as that of Si. Bonding and anti-bonding orbital at interfaces dominate the electronic properties. The free energy of surfaces and interfaces become a dominant factor for the formation of nanostructures. It determines the growth modes in thermal equilibrium.

The inherent size dependence of the macroscopic nanocrystal properties is the result of two primary mechanisms: free energy variation and quantum confinement [2]. Surface morphology of nanocrystals had been initially thought of as mostly disordered, but later work has shown that nanocrystals exhibit regular shapes with well-defined interfaces analogous to that of bulk

crystals. Nanocrystals thus have the ability to have their free energy manipulated in a controlled manner, correlated with particle size.

To summarize, reducing any piece of material from a shank that might be recognized to the nanometer scale changes virtually all of its most basic properties in a fundamental way. Its shape and crystalline structure change, as do its melting and boiling temperatures. Its magnetic properties also change [3]. Material properties change dramatically because quantum effects arise from the confinement of electrons and holes in the materials [4]. The dramatic changes in the properties of these materials due to miniaturization develop an interest in researchers in the field to dream about what to be done next. Nanoscience and nanotechnology emerge and begin to flourish with this essence.

UNIT-TWO

2. Nanotechnology

Nanotechnology is a catchall phrase for materials and devices that operate at the nanoscale. From the Greek 'nano' means "very small". In the metric system of measurements, 'Nano' equals a billionth (10^{-9}) of a unit and therefore, a nanometer is one billionth of a meter. In fact, the nanometer is the master unit for nanoscience and nanotechnologies. References to nanomaterials, nanoelectroics, nanodevices and nanopowders simply mean the material or activity can be measured in nanometers. To appreciate the size, a human red blood cell is about 2,000nm long. Virtually outside the nanoscale range [5]!

Nanotechnology deals with various structures of matter having dimensions of the order of a billionth of a meter. The scientific community generally attributes the first acknowledgment of the importance of the nanoscale range to the brilliant Nobel Laureate physicist Richard Feynman in his famous 1995 lecture "*There is plenty of Room at the bottom*" in which he first proposed that the properties of materials and devices at the nanometer range would present future opportunities [6]. The term reached greater public awareness in 1986 with the publication of "*engines of creation*"; "*The coming Era of nanotechnolgy*" by Drexler.

Feynman, in his visionary and prophetic lecture, speculated on the possibility and potentials of nano sized materials. He envisioned etching lines a few atoms wide with beams of electrons, effectively predicting the existence of electron beam lithography, which is used today to make silicon chip. He proposed manipulating individual atoms to make new small structures having very different properties. Many of Feynman's speculations have become a reality.

The fabrication of two dimensional quantum wells (1970s), first observation of quantum confinement (1982), the invention of STM and AFM electron-beam lithography, introduction of CNT (1990s) all put their contribution to the level of the present day nanotechnology

The distinct feature of nanostructured systems that distinguishes them from a bulk system needs to be understood from relevant length scale perspective. A rough sketch for their length and energy scale is given in fig. 3.1

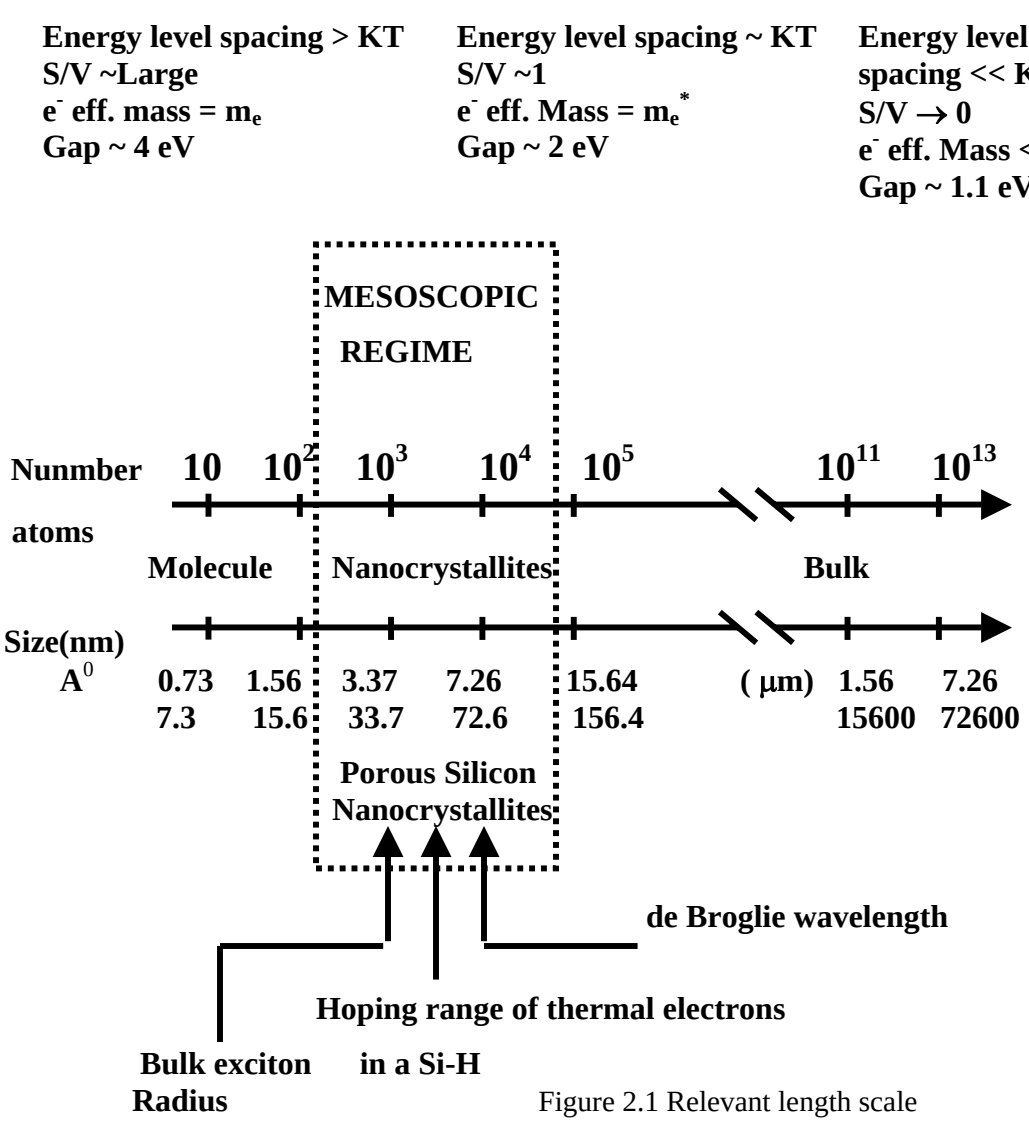

Figure 2.1 Relevant length scale

The area bounded by the dotted rectangle is the topically interested area called nanoscience. The structure may be in crystalline phase, porous phase, semisolid, or liquid

At nanoscale, surface forces become more prominent, quantum confinement effects and quantum excitations like excitons; polarons and polaritons become remarkably significant. It is these complex dynamics that controls all properties of a nanostructured system.

Recent scientific investigations have been made by studying nanaomaterials. It is now recognized that when matter is composed of only a handful of atoms new physics and chemistry begin to emerge. Nanotechnology of the future will utilize these existing processes in devices that cannot yet be imagined.

Despite the challenges due to its inter disciplinary nature, nano science and nanotechnology draws on the strength of all the basic sciences including physics, chemistry, biology, material science and engineering. Physics at nano scale, for instance, deals with CNTs, nanosilicon, hetero-structures, tailored materials, MEMS and NEMS nanoelectronics (powerful computers, small mobile phones, better digital cameras, audiovisual systems and so on).

Nanobiophotonics, nanobiosensors, nanoparticles, environmental monitoring and so on are some of the fields in nanoscience device application of which is revealed in nanotechnology.

To conclude, Nanotechnology is recognized as being the major technological revolution that billions of dollars are being spent worldwide in the race to develop nanodevices and nano materials. It is expected that break through in medicine and computer science will be instrumental in realizing the full potential of nanoscience and nanotechnology.

2.1 Bottom –Up versus Top-Down Approaches of Nanotechnology

There are a variety of techniques that are capable of creating nanostructures with various degrees of quality, speed and cost. These approaches fall under two categories – “bottom-up” and “top-down” [7].

Bottom-up manufacturing involves the building of structures, atom-by-atom or molecule-by-molecule. Chemical synthesis, self-assembly and positional assembly are three main approach in this method.

Top-down manufacturing involves treating with a larger piece of material and etching, milling or machining a nanostructure from it by removing material. This can be done using techniques such as precision engineering and lithography. The prime example of the top-down approach is seen in the development integrated circuits (ICs), where the feature sizes of the components have decreased from several microns to dimensions less than 100nm[13]. Well-known products with nanometer dimensions include digital versatile discs (DVDs) and DVD-players, sensors, security lights and ink jet printers.

A diagram illustrating some of the types of materials and products that these two approaches are used for is shown in fig.2.2.

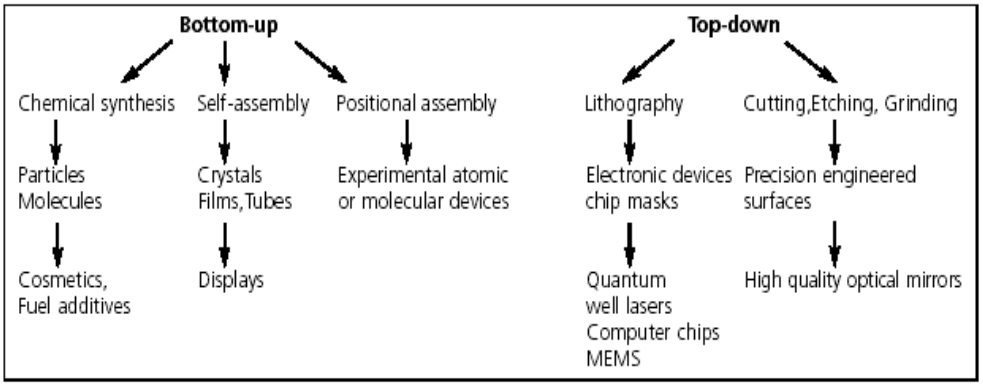

Figure 2.2 the use of bottom-up and top-down techniques in manufacturing

In recent years the limits of each approach in terms of feature size and quality that can be achieved, have started to converge. The relationship between top-down and bottom-up techniques is illustrated in fig 2.3. Now the dimensions that can be controlled by either approach are of a similar order, and this is leading to exciting new hybrid methods of manufacturing.

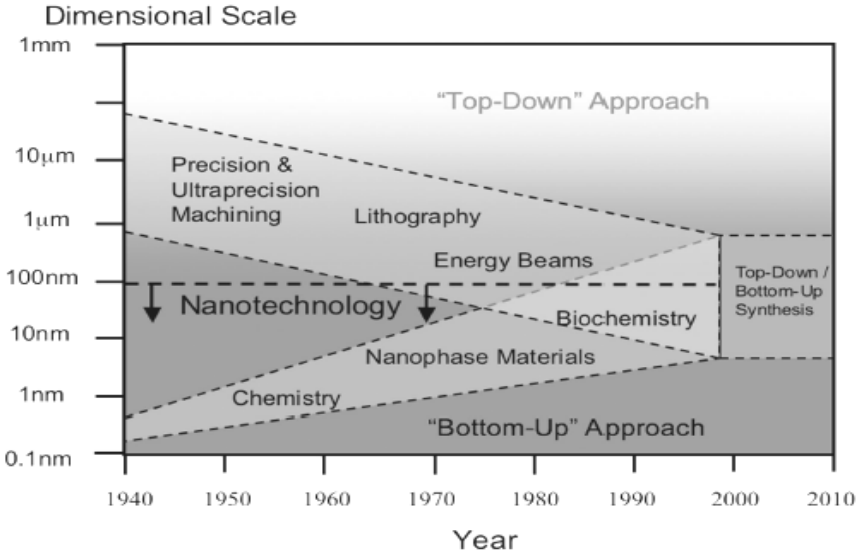

Figure 2.3 The convergence of top-down and bottom-up techniques (Whatmore 2001)

UNIT-THREE

3. Quantum Confinement and its Effects

Semiconductor nanocrystals having analogous interior bonding geometries compared to that of their known bulk counter parts exhibit distinct variations in their electrical and optical properties with size variation. The core reason for these changes lies in the systematic transformation of the crystal's density of states as a function of energy, which varies as function of the nanoparticles' interior. From a density of state perspective nanocrystals lie between discrete atomic and bulk "continuous band" limit. In any material, there will be a size below which one observes a fundamental shift in electronic and optical properties as a function of size [8]. This quantum size effect regime begins when the energy level spacing exceeds the temperature KT.

If we confine the electron hole pairs (excitons) in a small region, having dimensions of the order of a few nanometers, the properties of the material completely change. Since the order of magnitude of the electron and hole De Broglie's wave length (~1nm) is comparable with the confinement dimensions, they behave as particles in a box and the problem can be solved by quantum mechanics. Consequently, the confinement effect in a region of nanometric size is referred to as quantum confinement effect, and the physical structure, in which the quantum confinement of excitons occurs, is termed as a nanostructured material.

3.1 Quantum Dots, Quantum Wires and Quantum Wells

Progress in epitaxial growth and advances in patterning and other progressing techniques have made it possible to fabricate 'artificial' dedicated materials for microelectronics [9]. In these materials the electronic structure is tailored by changing the local material composition and by confining the electrons in nanometer size foils or grains.Due to the quantization of electron energies, these systems are often called quantum structures.

Quantum confinement of excitons may occur in only one direction, in two directions or in all the three directions depending on the shape of the nanostructures. At each confinement direction there corresponds a radical change in the wave function of the particle and as a consequence, a series of discrete levels appear.

Quantum Dot: - A quantum dot has all the three dimensions in the nano range. This means, there is a total confinement in each direction and particles cannot move freely anywhere. Thus it is referred to as a 0-D nanostructure.

Quantum Wire: - is a 1-D nanostructure where particles are free to move in only one direction. That is two sides of the structure are of nanometer length.

Quantum Well: - A quantum well is a nanostructure where there are two directions for the movement of particles, while the third direction determines the quantum confinement direction. It is said to be a 2-D nanostructure.

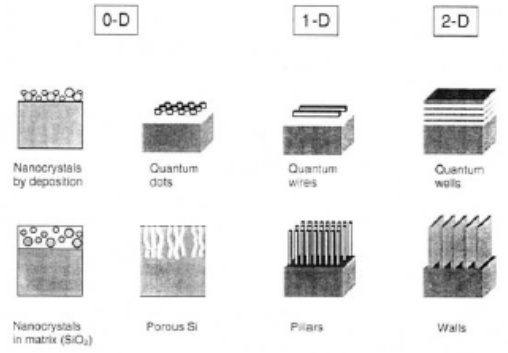

Figure3.1 Schematic of low dimensional Structure

Quantum dots can be obtained by means of different techniques such as chemical vapor deposition (CVD), Ion-implantation, sputter deposition, etc. 1-D structures (quantum wires) can be synthesized by depositing layers of different materials having nanometric dimensions; for example in $Si/Si0_2$ multipliers; $Si0_2$ layers act as a barrier, while excitons are confined in the Si layers. Fig (3.1) gives the nanostructures classification in different dimensions.

3.2 Density of State (DOS) in View of Quantum Confinement

As a result of quantum confinement in different directions, there is a change in the wave function describing the behavior of electrons and holes, and consequently also the number of states per unit energy, i.e., the density of states (DOS), changes as a function of the energy E of the particle. On the other hand, the arrangement of the atomic bonds at the surface also strongly affects the energy distribution of electronic states, since in Si-nc the silicon atoms are at the surface or few lattice sites away [8]. Figure 3.1 gives the schematics of the low dimensional structures.

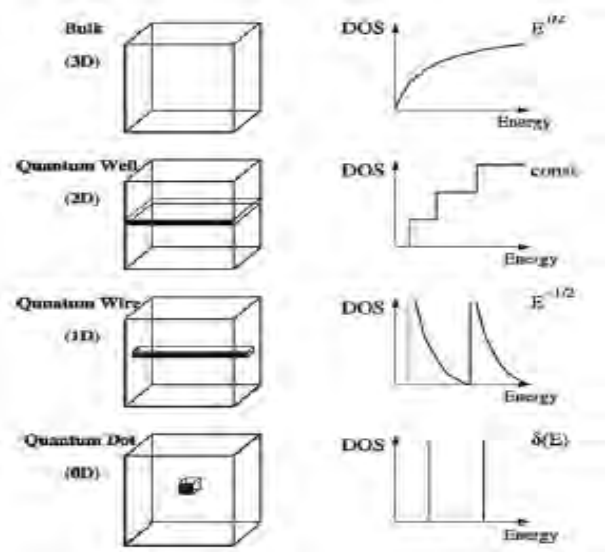

Figure 3.2 the density of states as a function of energy for a particle confined to move in the bulk, in a q.well, q.wire, and q.dot

In the case of a bulk material, the density of states increases with the energy of the particle following a parabolic law, the DOS being proportional to $E^{1/2}$. Quantum confinement in one direction determines a step like increase of the DOS function with the energy. Totally different is the DOS function in the case of a 1-D nanostructure where the number of states decreases following $E^{-1/2}$ law as the energy increases. In the case of 0-D structures, the function in the ideal case is formed by deltas marking the presence of discrete levels as indicated in fig. 3.2

Since the density of states as a function of energy varies with a transition from the atomic to bulk crystal regime, it logically follows that both optical and electronic properties depend strongly on nanocrystal size. The energy required to add successive charges on to an extended (bulk) crystal does not vary. In nanocrystals, however, the presence of one charge acts to prevent the addition of another. Thus, in metals or semiconductor, the current-voltage curves of individual crystallites resemble an additive step function- a staircase. This effect is often termed as "Coulomb blockade" [2]. Step in the staircase due to individual charging events are spaced proportional to the reciprocal of the particle radius.

3.3 Energy Gap of Nanostructures

Most of a material's behaviors, such as intrinsic conductivity optical transitions electronic transition, depend on the energy-gap between the conduction bands (CB) and the valance

band (VB). Any change of the gap may significantly alter the material's physics and chemistry. Miniaturizing a semiconductor for instance down to a nanometer scale causes the band gap (E_g) to expand and the inner core level to shift towards higher binding energy. The dielectric constant ε_r of the semiconductor is no longer constant but decreases with solid size. The reduced ε_r has enormous impact on the electrical and optical performance of the solid and the related devices [10]. This occurs when the width of a solid is reduced to the nanometer length scale.

In addition to the size, effects such as structural changes, lattice contractions, surface passivation, atomic relaxation, surface reconstruction and strain induced by a host material can change the gap. Figure 3.3 compares the energy gap of bulk silicon with that of the nanocrystal structure of silicon.

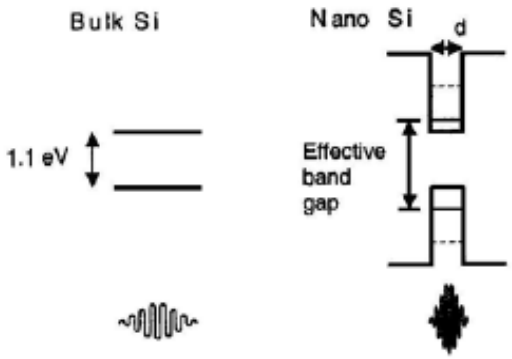

Figure 3.3 The increase of the band gap with decreasing crystalline size due to quantum confinement

The quantum size effect predicts the formation of a band gap with decreasing particle for metals, and widening of the intrinsic gap for semiconductors.

Silicon nanocrystals, for instance, are complex systems and several models have been proposed in order to describe their band structure. The simplest model used to describe the band gap in such nanostructures or quantum dots is the effective mass approximation (EMA) [8]. By using this model a Si-nc is thought as a spherical potential well that bounds an exciton by means of a high and wide potential barrier determined by the SiO_2 matrix.

There is non-negligible amount of negative Coulombic attraction between the electron and its associated vacancy (hole). Although free excitons are free to move about the crystal as an e-h pair, as long as sufficient optical excitation continues the electron and the hole will both be

mutually bound. That is, free electrons are still bound as e-h pairs. Of course, there is a natural spatial e-h separation most desired by the system. In the EMA approximation, this separation used to establish the presence of quantum confinement effect, is the Bohr radius of the exciton. This may be easily calculated by balancing the central force on the electron (m_0v^2/r_n) to the Coulombic attraction force $\left(\frac{q^2}{4\pi\varepsilon_0 r_n^2} \right)$

$$\text{i.e., } \frac{m_0 v^2}{r_{ex}} = \frac{q^2}{4\pi\varepsilon_0\varepsilon_r r_{ex}^2} \quad \ldots\ldots\ldots\ldots\ldots\ldots\ldots\ldots\ldots\ldots \quad (1)$$

Via the Bohr postulate, the angular momentum L may be expressed as $m_0 v r_n = n\hbar$

$$\text{It follows then; } r_{ex} = \frac{4\pi\hbar^2\varepsilon_r\varepsilon_0}{\mu e^2} \ldots\ldots\ldots\ldots\ldots\ldots\ldots\ldots\ldots\ldots\ldots\ldots\ldots\ldots \quad (2)$$

Where μ is the reduced mass of the exciton, e is the electric charge of the electron, ε_r is the relative dielectric constant of Si, ε_0 the dielectric constant of vacuum and h is plank's constant. Table1.gives calculated excitonic Bohr radii for various materials

Material	Excitonic Bohr Radius
Cadmium sulphide	315
Zinc Sulphide	50
Lead Sulphide	204
Lead Selenide	460
Cadmium Selenide	61
Silicon	55
Zinc Oxide	18
Copper Chloride	10
Indium Arsenide	340
Indium Antimonide	540
Cadmium Telluride	100

Table 1. Calculated excitonic Bohr radii for various metals

The significance of the excitonic Bohr radius is that it provides a threshold value below which the confinement regime becomes relevant. That is, an exciton in a nanoparticle will

not experience confinement if it is restricted to a spatial dimension larger than that of its own preferred electron-hole spatial separation.

Effective mass approximation can be illustrated by a simple case of confinement in a nanocrystal with linear dimension L_x, L_y, Lz where the band gap is given by the expression:

$$E_{nc} = E_{Si\text{-}buck} + \frac{h^2\pi^2}{2}\left(\frac{1}{m_e^*}+\frac{1}{m_h^*}\right)\left(\frac{n_x^2}{L_x^2}+\frac{n_y^2}{L_y^2}+\frac{n_z^2}{L_z^2}\right) \quad \text{..... (3)}$$

Where $E_{Si\text{-}bulk}$ = 1.lev, while m_e^* and m_h^* are respectively the effective mass of electrons and holes. According to this expression, it is evident that the energy necessary to generate an electron-hole pair increases by decreasing the size of the system. Theoretical calculations of the band-gap widening have been confirmed experimentally by absorption measurements [11]. Figure 4.4 illustrates the calculated band-gap variation with a decrease in size of the particles. Experimental band gap data from photoemission and photoluminescence studies as well as pseudo-potential calculation are given in figure 4.5

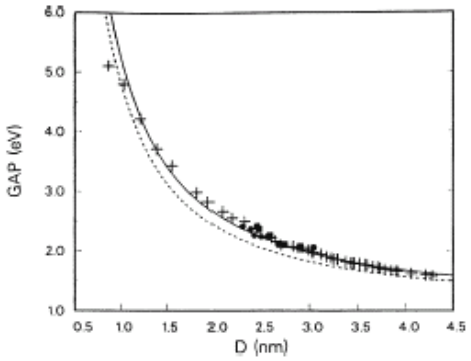

Figure 4.4 Calculated optical gap energies for Si-crystals depending on their diameter

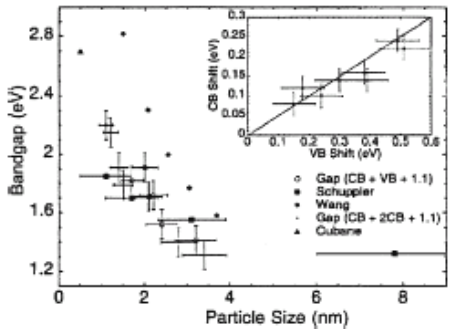

Fig. 4.5 Band gap of Si-particles as a function of particle size

Because of the finite number of atoms and the quantum confinement, the energy bands of a nanocrystal are split into discrete levels, which widen as the radius of the nanocrystal decreases as illustrated in figure 4.6a.To a first approximation, for a spherical nanocrystal the energy gap E_g is given by:

$$E_g = E_{g,bulk} + \frac{\hbar^2\pi^2}{2r^2}\left(\frac{1}{m_e^* m_e}+\frac{1}{m_h^* m_e}\right) - \frac{1.8e^2}{4\pi\varepsilon\varepsilon_0}\frac{1}{r} \text{..... ..... (4)}$$

where the first term Eg, $_{bulk}$ corresponds to the gap of the macroscopic crystal [13]. The second $\frac{1}{r^2}$ term, called quantum confinement, is calculated assuming a spherical nanocrystal in which are confined an electron and a hole of respective effective masses $m_e^* and m_h^*$. The effective mass is a corrective factor applied to the mass of the free to allow for the curve of the valence and conduction bands near the energy gap. The last term accounts for the Coulomb attraction between the electron and the hole. Quantum confinement increases the gap as r decreases, more steeply with a smaller r (variation with r^{-2}). This situation is depicted in figure 3.6a.

Equation 4 gives E_g for nanocrystals of different semiconductors from macroscopic solid parameter (fig.3.6b) With appropriate light excitation, nannocrystals can re-emit, by fluorescence, photons of energy equal to the gap value [13].

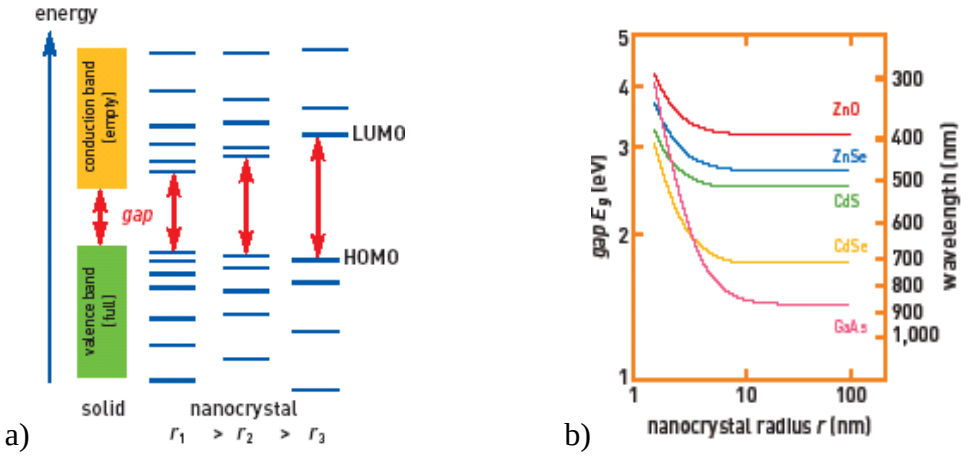

Figure 3.6 a) Schematic evolution of the electronic structure between the macroscopic solid and nanocrystal of decreasing size. b) Theoretical variation of the gap calculated from the equation for the nanocrystals of different semiconductors.

In addition to the variation of the energy spectrum, also the wave functions of the electron and the hole are influenced by the quantum confinement in the dot [14]. Overlap of the wave functions in real space and spreading of them in the K-space causes an increase in the optical transition as shown in Figure 3.7.

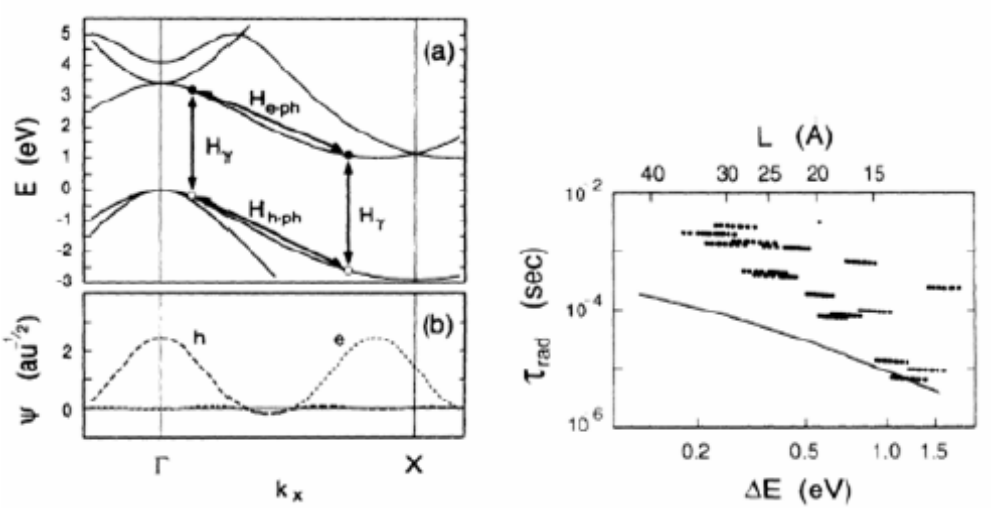

Figure 3.7 Spread of the electron and hole wave function in a quantum dot (left) and calculated radiative lifetime versus size for Si-quantum dots (right).

Semiconductor nanocrystals encounter a distinct large magnitude change in their optical properties as a function of nanoparticle size. With a reduction in size, the quantized density of states near the band edges shifts to a higher energy. Optical activity is concentrated to just a few transitions, resulting in an enhancement in nonlinear optical effects.

The change in the density of available electronic states are understood by initially considering Heisenberg's uncertainty relationship (Eqn.5) between momentum and spatial positioning of both free and confined particles.

$$\Delta P_x \Delta X \geq \frac{\hbar}{2} \quad \text{..... (5)}$$

For a free particle or one that is confined to a periodic potential, the energy and the momentum may be well defined, but simultaneously the particle position is not defined. Localization of the particle to within a particular restricted range results in a decrease in the momentum certainty but a simultaneous increase in the position certainty. The momentum uncertainty (i.e. the superposition of bulk states) and spatial localization resulting from confinement are inversely proportional in the Heisenberg relation. Coupling the uncertainty with the energy dependence on the square of the wave vector leads directly to the approximate dependence of energy on size as the inverse of r^2 analysis, where energy is also proportional to the inverse of r^2 .The dependence of energy on well width has a direct consequence on the variation of optical properties with nanocrystal size.

3.4 Recombination Process in Crystalline Silicon

The luminescence from a semiconductor is generally the result of electron-hole pair radiative recombination. The photon energy is equal to the energy released in the recombination. Since photon momentum is negligible, its emission requires either direct recombination or generation (absorption) of a phonon for momentum conservation [8]. Semiconductors are, therefore, commonly divided in to two distinct categories depending on the nature of their band gap (figure 3.8)

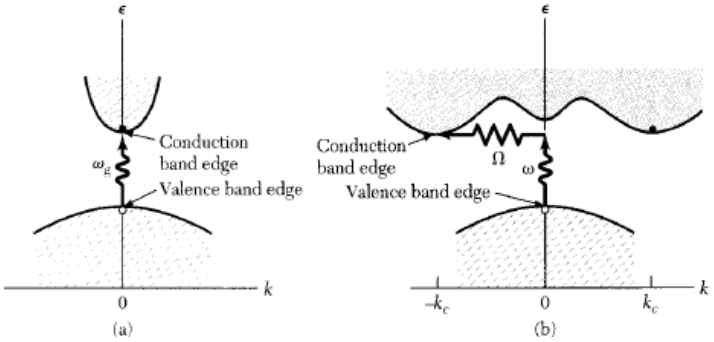

Figure 3.8 Schematic of the direct and indirect band gaps of semiconductors.

In direct band-gap semiconductor the minimum of the conduction band and the maximum of the valence band are coincident in the K-space of the crystalline momentum (e.g. GaAs). On the other hand, silicon has an indirect band-gap and the maximum of the valance band and the minimum of the conduction band appear not to coincide.

Thus, radiative recombination in silicon requires a phonon, which significantly reduces the probability and rate of these processes. The radiative lifetime is given by:

$$\tau_{rad} = \frac{1}{B(n_0 + \Delta n)} \quad \text{..... (6)}$$

Where B is the coefficient for radiative recombination, n_o the dopant density for p-type or n-type material and Δn the injected carrier density.

At the same time there are competing non-radiative processes, such as Shockley-hall-read (SHR) recombination through deep traps due to the presence of defects or impurities in the crystal, characterized by minority carrier lifetime in the low injection regime given by:

$$\tau_{nrad} = \frac{1}{N_T v_{th} \sigma_T} \quad \text{..... (7)}$$

Where N_T is the density of traps, v_{th} is the thermal velocity of the minority carriers and σ_T is the capture cross-section for the minority carries

The lifetime for the non-radiative (SHR) recombination is much shorter than the radiative recombination life time for e-h pairs in silicon, indicating that non-radiative recombination are much more probable [8].

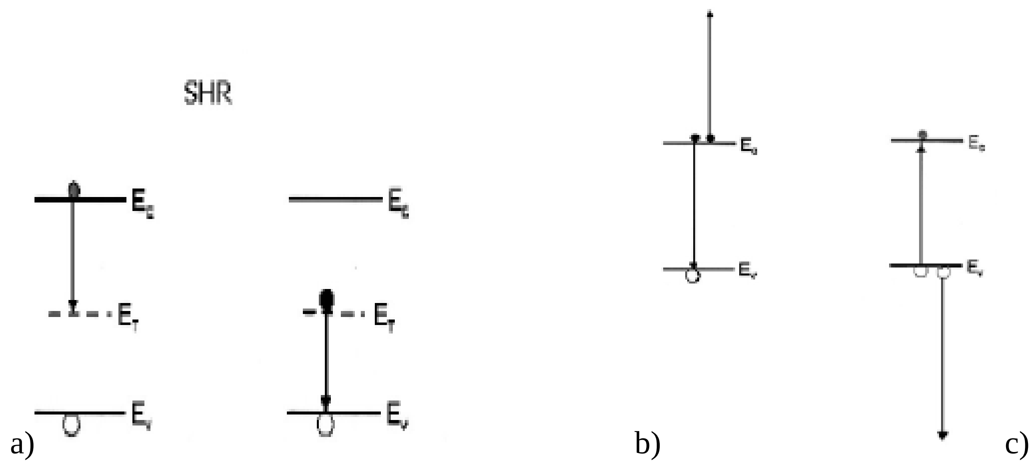

Figure 3.9 a) Recombination /generation process of e-h pairs in crystalline silicon by means of Intermediate trap centers. b) and c) Auger recombination process involving free carriers (eeh or ehh).

Furthermore, in heavily doped silicon, e-h pairs can recombine through Auger processes. In Auger recombination the energy of the e-h pair is given to a third particle such as an electron (eeh Auger recombination for n-type Si) or a hole (ehh Auger recombination for p-type Si). Non-radiative Auger recombination provides the fastest de-excitation path.

The lifetime τ_{Auger} for an Auger processes is determined by;

$$\tau_{Auger} = \frac{1}{c_p p_0^2} \text{ or } \tau_{Auger} = \frac{1}{C_n n_o^2} \quad \ldots\ldots (8)$$

Where C_p and C_n are the Auger coefficients for the ehh and eeh and P_o and n_o are the dopant concentration. Since all the different recombination processes described above act in parallel, the total lifetime is given by:

$$\frac{1}{\tau} = \frac{1}{\tau_{rad}} + \frac{1}{\tau_{SRH}} + \frac{1}{\tau_{Auger}} \quad \ldots\ldots (9)$$

and the quantum efficiency is:

$$\eta = \frac{\tau_{nonrad}}{\tau_{nonrad} + \tau_{rad}} \quad \ldots\ldots (10)$$

Where τ_{nonrad} is the lifetime for the non-radiative processes.

In summary, the quantum confinement effects in nanostructures result in the descretization of the density of states as a function of energy. Subsequently, the electrical and optical properties of the material change drastically.

UNIT-FOUR

4. Bulk Silicon

Silicon (Si) is the chemical element in the periodic table with atomic number 14. It is the second most abundant element next to oxygen in the earth's crust in nature.

It occurs most often as oxides and as silicates. Sand, amethyst, agate, quartz, rock crystal, fling, jasper, and opal are some of the forms in which the oxide appears. Granite, asbestos, feldspar, clay, hornblende and mica are a few of the many silicate minerals similar to other group IV elements [15]. Silicon easily forms four covalent σ bonds in tetragonal coordination (sp^3 hybridization) and typically crystallizes in a diamond like structure.

4.1 Production: Silicon is commercially prepared by the heating of high purity silica in an electric arc furnace using carbon electrodes [16]. At temperatures over 1900^0c, the carbon reduces the silica to silicon according to the chemical equation:

$$SiO_2 + C \longrightarrow Si + CO_2$$

4.2 Characteristics and Structure: - This crystalline form silicon has a metallic luster and a grayish color. Even though it is a relatively inert element, silicon still reacts with halogens & dilute alkalis, but most acids (except for a combination of nitric acid and hydrofluoric acid) do not affect it [15]. Silicon is a semiconductor with a diamond lattice structure. Due to its unique electrical properties, it is the most important technological material in electronics industry. The crystal structure of crystalline silicon is illustrated in figure 4.1 [17].

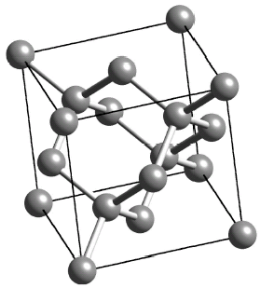

Figure 4.1 Diamond crystal structure for elemental silicon

4.3 Purification: - The use of silicon in semiconductors devices demands a much greater purity than afforded by metallurgical grade silicon.

The chemical method of purification is one of the methods used to produce high purity silicon. In this method silicon is purified by converting it to a silicon compound that can be more easily purified than silicon itself, and then converge that silicon compound back into

pure silicon. Trichlorosilane is the silicon compound most commonly used as the intermediate, although silicon tetrachloride and silane are also used. When these gases are blown over silicon at high temperature, they decompose to high purity silicon. In the siemens process, high purity silicon rods are exposed to trichlorosilane at 1150^0c. The trichlorosilane gas decomposes and deposits additional silicon on to the rods, enlarging them according to chemical reactions like;

$$2H\ \ Si\ CL_3 \longrightarrow Si + 2HCL + Si\ CL_4$$

Silicon produced from this and a similar process is called polycrystalline silicon. Bulk silicon is the material of choice for microelectronics fabrication. It is an indirect band gap semiconductor with a centro symmetric crystalline structure. As a result bulk silicon is not directly suited for optoelectronics. The indirect band gap makes light emission by free carrier recombination extremely unlikely; whilst the lattice symmetry results in the lack of electro-optic effect. More over the bulk silicon band gap of 1.16eV prevents its use for light detection at the technologically important 1.3 and 1.55 μm.

As a consequence of its indirect band gap, bulk silicon has a typical room temperature quantum efficiency of < 0.001% compared to around 1-10% for GaAs LEDS and around 30% for specialized GaAs and InP devices [18]. This poor efficiency results primarily from the fact that the lowest energy transition (figure4.2b) violates conservation of momentum and therefore requires phonon assistance. Consequently, the exciton lifetime is very long and non-radiative recombination dominates the relaxation process. In nanoscale structures, the requirement for momentum conservation is relaxed and the probability for direct transmission is increased.

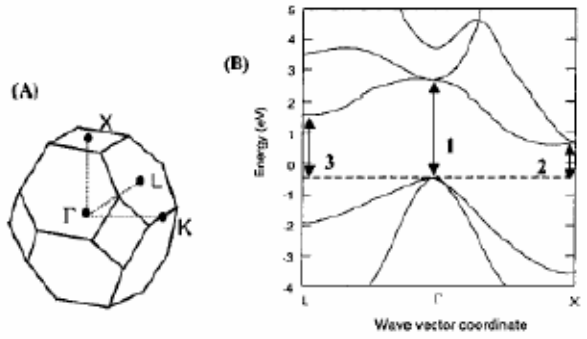

Figure 4.2 a) Brillouin zone for the diamond lattice, and b) bulk band structure of Si. The arrow in b) indicate the energies of the direct (1) and indirect phonon assisted transitions $\Gamma \rightarrow X$ (2) and $\Gamma \rightarrow L$ (3).

4.4 Applications: - Silicon is a very useful element. Silicon dioxide in the form of sand and clay is an important ingredient of concrete and brick and is also used to produce portal and cement. Silicon is a very important element for plant and animal life. Diatoms extract silicon from water to build their portative cell walls.

Other applications include:

- Pottery /Enamel- It is a refractory material used in high temperature material production and its silicates are used in making enamels and pottery
- Steel- Silicon is an important constituent of some steels
- Abrasives- Silicon carbide is one of the most important abrasives
- Semiconductor- Ultra pure silicon can be doped with arsenic, boron, gallium or phosphorus to make silicon more conductive for use in transistors, solar cells and other semiconductor devices.
- Construction- Silicon is a major ingredient in bricks because of its low chemical activity
- Medical material- Silicones (not silicons) are flexible compounds containing silicon-oxygen and silicon-carbon bonds; they are widely used in applications such as artificial breast implants and contact lenses.

UNIT-FIVE

5. Porous Silicon (p-Si)

The construction of nanocrystals with strong photoluminescence (PL) in the entire optical range, have astonished the whole community of solid-state scientists. An important goal was the discovery of strong PL porous silicon, which constituted a very easy and economic way for having high performance PL silicon structure. In this chapter, we discuss the formation and different properties of this material.

Porous silicon is a form of chemical element silicon, which has an extremely large surface to volume ratio [19]. Among the many different Si-based materials studied for their luminescence properties, porous silicon (p-Si) has proved to be one of the most promising, as it emits light at room temperature in the visible range with quantum efficiencies approaching 10% (one photon emitted for every 10 photon-generated e-h pairs) [20].

Porous silicon was discovered by Uhlir (1956) but its luminescence properties remained unnoticed until 1990, when L.T Canham reported them. Certain p-Si materials can have large photoluminescence efficiency at room temperature; a surprising result, since the PL efficiency of bulk silicon is very low due to its indirect energy band gap and short non-radiative lifetime. The reason of this was the partial dissolution of silicon, which causes:

i) The formation of small silicon nanocrystals in the porous silicon material,

ii) The reduction of the refractive index of p-Si with respect to silicon, and hence an increased light extraction efficiency from p-Si and

iii) The spatial confinement of the excited carriers in small silicon regions where non-radiative recombination centers are mostly absent.

The word *nanoporous* is sometimes used for smallest-pore regime to emphasize the nanometric dimension [21]. The volumetric fraction of air of the material is called porosity (P). The internal surface of p-Si per unit volume can be very large, of the order of 500 m^2/cm^3.

5.1 Fabrication Procedure

P-Si is mostly fabricated by electrochemical anodization — often referred to as electrochemical etching — of bulk Si wafers in diluted aqueous or ethanoic hydrofluoric acid (HF). Typical anodization arrangements are schematically shown in Figure6.1. The anodization is performed in a galvanostatic (current –controlled) mode.

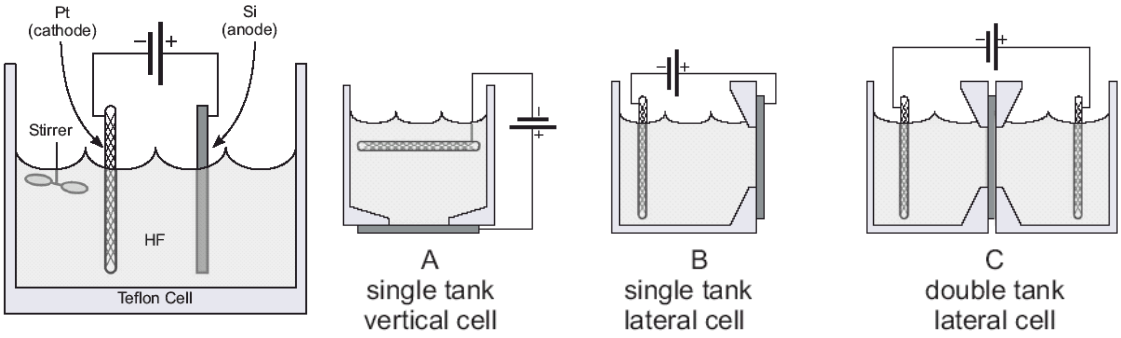

Figure 5.1 Schematic anodization arrangements: Principle (right) and practical examples (A, B,and C).

Platinum and Teflon are mostly used because of their chemical resistance to HF. In the practical arrangements A B and C, the Si area exposed to the solution — typically about 1 cm, circular — is well defined by the Teflon cell. Rubber gaskets between Si and Teflon can easily avoid spills. Type A is easier to design, type B is convenient when Si illumination is desirable (for example, for n-type Si,) type C does not require electrical contacts on Si [21]. An optional stirrer is sometimes used to improve diffusion of HF during the anodization.

To form p-Si, the current at the Si side of the Si/electrolyte interface must be carried by holes, injected from the bulk towards the interface. The current must be kept between zero and the electro-polishing threshold, which can be identified as the value of the first maximum of the anodic regime in the I-V curve. In order to achieve significant hole current in n-type Si, external illumination of the sample is required, depending on the doping level. If the current exceeds the electro-polishing threshold, the anodization results in a progressive, complete removal of Si. The wafer has then a mirror-like appearance.

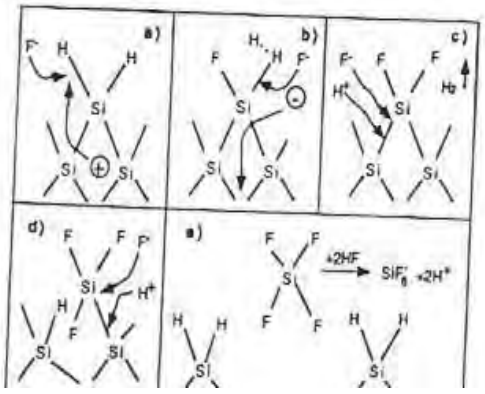

Figure 5.2 The reaction mechanism for p-Si formation

A hypothesized chemical reaction, which could describe the anodization, is:

$$Si + 6HF \longrightarrow H_2SiF_6 + H_2 + 2H^+ + 2e^-$$

The last term — a negative charge at the interface, to be neutralized by the current flow — would explain the need of hole injection from the substrate towards the Si/electrolyte interface.

At the Si/electrolyte interface a depletion zone is formed. The width of this depletion zone depends on the doping and may explain the different pore sizes found in p- and p+ type doped silicon. For hole depletion at the surface of the attacked wafer two mechanisms are thought to be responsible. The first is quantum confinement effect which occurs when feature size decreases below the dimension of the Bohr radius of an exciton (~5nm) .The second is the formation of a depletion layer due to the Si electrolyte constant.

The quantum confinement effect yields micro porous Si, when the depletion layer is thin, holes tunnel from Si to electrolyte, this leads to the formation of mesopores, with thicker depletion layers break down is responsible for charge transfer [20,21]. In addition, the depletion layer width depends on the surface curvature: the anodization preferentially occurs at the pore tips where the curvature is largest. Figure 5.3 illustrates the steps undertaken in the process.

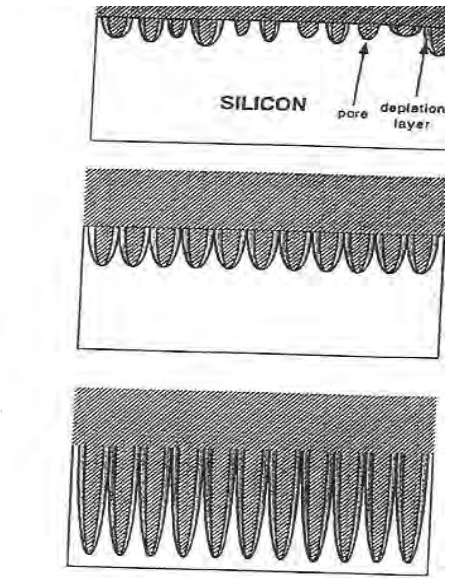

Figure 5.3 Steps in p-Si formation: a) pores are formed at the surface of the Si wafer, b) their Walls are thinned until they are depleted of holes; c) the reaction proceeds at the pore ends.

Moreover, when the depletion zones of adjacent pores meet each other, the current flow is suddenly pinched off. Further Si etching is blocked, and pore collapsing is prevented. For this reason the reaction is self limited in the hashed anodization regimes of Figure 5.5 and leads to a porous structure rather than to electro polishing. As further practical consequence, in stationary conditions, the porosity remains approximately constant, whereas the overall thickness of the p-Si layer grows essentially linearly in time. The etching process leads to a very regular pore growth, which is most effectively exploited to fabricate macro porous photonic crystal devices (Figure 5.4).

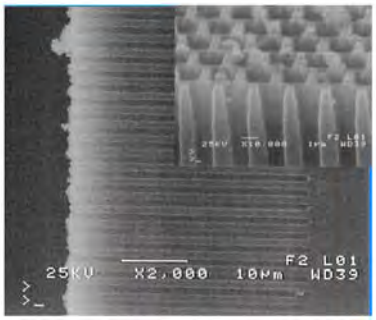

Figure 5.4 Example of a photonic crystal (cross-section an top-view images of the same sample) realized with ordered macro porous P-Si in a p-type doped substrate. This photonic crystal has a photonic band gap at 3.5 μ m

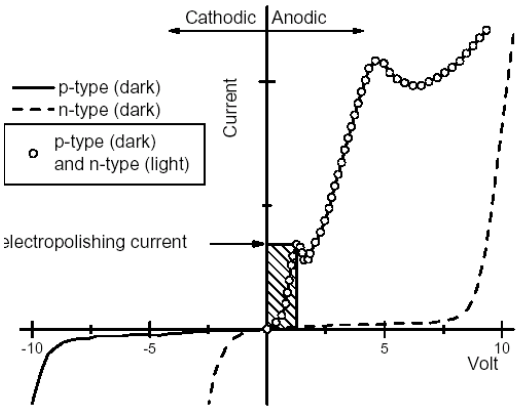

Figure 5.5. Typical I-V characteristics of an electrochemical cell for P-Si fabrication

The hashed region in figure 5.5 corresponds to the useful regime where p-Si can be achieved, assuming the I-V characteristic marked with hollow circles. In the anodic regime, the characteristics of a cell with n-type Si will lay in the region bounded by the characteristic in dark (dashed line) and in full light (hollow circles) [21].

To avoid extended cracking due to large capillary stress, a drying technique such as pentane drying is employed. Immediately after drying p-Si, hydrogen surface passivation is gradually replaced by native oxide. This chemical change affects most p-Si properties. To stabilize p-Si properties oxidation is often used. Oxidation implies the formation of a layer containing the original Si atoms. Therefore, it also reduces the nanocrystallite size, with remarkable impact on photoluminescence emission energy (blue-shift). The employment of controlled oxidation procedures is therefore a valuable post-anodization option towards a better control of p-Si properties and stabilization.

To summarize, the main requirements for p-Si formation are:

1. The silicon wafer must be anodically biased. This corresponds to forward biasing for p-type Si, and reverse biasing for n-type Si.
2. In the case of n-type and semi-insulating p-type Si, light must be supplied
3. Current densities below critical values must be used.

5.2 Structure of Porous Silicon

Structural properties of p-Si have been investigated by Electron microscopy, Scanning probe microscopy, X-ray scattering techniques, X-ray absorption techniques, and Raman spectroscopy. In particular, X-ray absorption spectroscopy can be performed not only by extended X-ray absorption fine structure (EXAFS) analysis, but also by X-ray excitation of optical luminescence (XEOL), a convenient tool for luminescent sample, in which absorption is probed via the measurement of the corresponding optical emission. A general feature resulting from the comparison of these techniques is that highly luminescent p-Si is a composition of variously connected silicon crystals of nanometric dimensions (typically, 1 to 5 nm in radius). Smaller sizes than Si Bohr radius ($\approx$4.9 nm) imply significant quantum confinement effects. Raman measurements are also often used to demonstrate crystallinity in p-Si skeleton and infer information on the size of Si nanocrystals.

The p-Si structure obtained is of a layer made up of voids and nanocrystals inter-connected by an amorphous matrix, (Fig.5.6). In general, porous silicon is an inter-connected network of air holes (pores) in silicon.

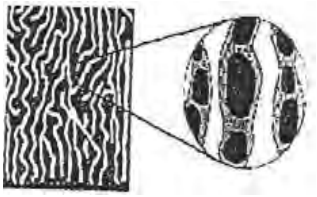

Figure 5.6 Model of a porous silicon structure

Both experiment and theoretical studies conducted recently seem to indicate that short-range crystallinity, passivation and confinement combine to produce p-Si luminescence.

Porous silicon is classified according to the pore diameter; which can vary from a few nanometers to a few microns depending on the formation parameter. P-Si is, therefore, classified as nanoporous (pore size less than 5nm), mesoporous (pore size of 5-50nm) or micro porous (with a pore size greater than 50nm). Figure .7 illustrates the different porous silicon structures of different pore diameter [10].

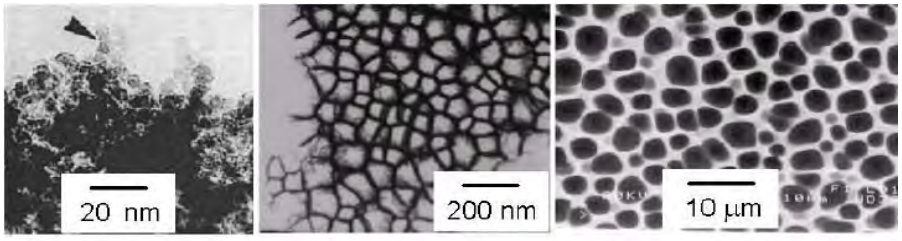

Figure 5.7 Examples of p-Si structures: nano porous (left), mesoporous (center) and macro porous (Right).

EPR measurements were used to study the paramagnetic defects in p-Si. Dangling bond type defects have been observed at the interface between the pore walls and an oxidized layer, and are thought to act as non-radiative recombination centers [20]. The model of p-Si, which emerges from these results, is of a layer made up of voids and nanocrystals interconnected by an amorphous matrix.

Porous silicon is usually mono-crystalline but evidence for amorphous regions has been found using X-ray scattering, X-ray absorption fine structure, Raman spectroscopy and electron microscopy [22].

5.3 Properties of Porous Silicon

5.3.1 Photoluminescence (PL)

Photoluminescence is a powerful, non-destructive technique for measuring the optical properties of a sample. It is the spontaneous emission of light from a material under optical excitation. A laser beam is directed on to the sample and, if of sufficient energy, photons are absorbed and electronic excitations is created. Eventually, these excitations relax and the electrons return to the ground state. The relaxation can occur radiatively with the emission of

a photon or non-radiatively through Auger recombination or defect related relaxation [18]. PL measures the radiative recombination and as such is a sensitive probe of electronic states.

P-Si exhibits efficient room temperature luminescence in the visible range. The complexity in the structure of this material has led to the formation of many different models to explain its luminescence. Basically, they can be grouped into three categories:

1. Quantum recombination model
2. Surface state model
3. Molecular recombination model

The first two models agree on the fact that quantum confinement plays a fundamental role in p-Si luminescence but they differ in their predictions about the origin of the luminescence.

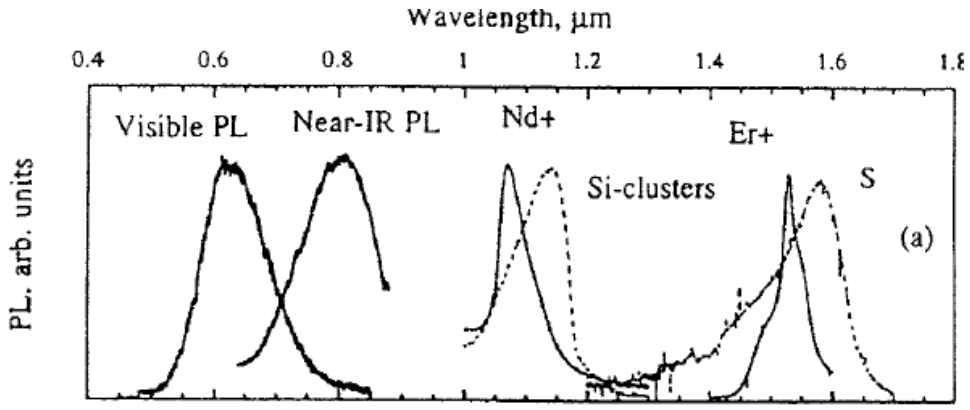

Figure 5.8 Room temperature photoluminescence spectra for various P-Si structures which have been oxidized or implanted with some selected impurities.

The former model ascribes it to the recombination of excitons with in the nanocrystals, where as in the latter individual (i.e., not coupled) charge carriers which could be found either in a bulk nanocrystal state (extended state) or trapped in a surface nonocrystal state, recombine radiatively. According to the third model, molecular species such as polysilane chains or siloxene rings are present in the amorphous phase of p-Si and are responsible for the luminescence (fig-5.8)

P-Si luminescence is thought to originate from excitons recombination in quantum dots structures. Because of confinement, the exchange energy between triplet and singlet exciton states increases. In crystalline silicon it is roughly 0-1meV, where as it becomes of the order of 10meV in p-Si.

Recombination from the triplet state ($(\uparrow\uparrow)$) is a forbidden transition, with decay time of the order of milliseconds, while that from the singlet state ($\uparrow\downarrow$) is allowed and has decay times in microsecond range.

When e-h pairs are formed in the nanorystals, they relax to the quantum dot's fundamental energy level on a fast time scale. At low temperature, practically all exciton will find themselves in triplet states, while the occupation of singlet states will increase with increasing temperature. Consequently the temperature dependence of the radiative lifetime (τ_{rad}) results from the thermal equilibrium between the exciton occupation of the triplet and singlet states [20]. The radiative lifetime as a function of temperature and energy is given by:

$$\tau_{rad}(E,T) = \left\{ \frac{1+(1/3)\exp(-\Delta E_x / K_B T)}{1+(\tau_{trip}/\tau_{\sin g})(1/3)\exp(-\Delta E_x / K_B T)} \right\} \quad \text{..... (11)}$$

Where $\tau_{\sin g}$ and τ_{trip} are radiative life times for the singlet and triplet states respectively, and ΔEx is the energy.

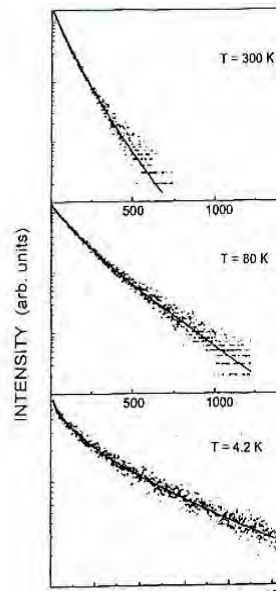

Figure 5.9 Time decay of the luminescence of a 60% porosity sample at three temperatures.

After excitation the e-h pairs are involved in one of the following processes:

i) Recombination in the quantum dot of origin through radiative channel.

ii) Recombination through non-radiative channel.

iii) Diffusion to neighboring quantum dots.

In conclusion, many aspects of p-Si luminescence are well described in terms of exciton recombination in quantum dots. Disorder plays an important role in the process, and rules the motion of excitons between quantum dots as explained by the trap-controlled mechanism.

5.3.2 Chemical Properties

Surface chemical composition of p-Si is best probed with Fourier Transform Infra Red (FTIR) spectroscopy. FTIR signal in p-Si is larger and easier to measure than in bulk Si due to much larger specific area. In fresh, as-prepared samples, oxygen is normally absent, the dominant bonds being Si-H groups (x = 1, 2 or 3). Ageing is observed as a slow replacement of H by O bonds in p-Si. Also luminescence fatigue is explained by photochemical reactions occurring on the surface of the Si nanocrystals.

5.3.3 Electronic Properties

The first and most favorable explanation for the visible emission in p-Si is the quantum confinement of excitons in nanometer-sized silicon.

An empirical law, based on the effective mass approximation, links the energy gap E_g of silicon nanocrystals with their sizes. The energy gap opening is given by an equal energy shift of the bottom of the conduction band to high energy and of the top of the valence band to low energy [21]. The nature of the energy-gap is still indirect even though a quasi-direct band gap can be formed in ultra small Si- nanocrystals.

5.3.4 Electrical Properties

Electrical resistivity in p-Si is five orders of magnitude higher than in intrinsic Si, because p-Si is depleted by free carriers. Depletion can occur either because of the energy gap widening from quantum confinement which reduces the thermal generation of free carriers, or because of trapping of free carriers. Trapping can occur during the preparation of p-Si either because the binding energy of dopant impurities are increased or because of the formation of surface states. It has been demonstrated that the dopants are still present in essentially unchanged concentration after the etching, but are in a neutral state. The electrical transport is mainly affected by the disordered structure of the Si skeleton, which restricts the conductive paths to a highly constrained geometry, which for certain porosities forms percolated or fractal geometry. As a consequence conductivity is thermally activated, strongly frequency dependent and highly dispersive.

For a nanocrystalline p-Si layer obtained by an electrochemical etching the current–voltage (I –V) characteristics at room temperature (RT) and the current–temperature (I – T) ones were taken using a Keithley 642 electrometer, a Keithley 2000 multimeter, and an Agilent E3631A d.c. power supply. Fresh p-Si samples have a slow rectifying behavior in the whole voltage range. On the contrary, the oxidized samples have a strong rectifying behavior (Figure5.10a). Up to 2.2V in forward bias the curve is exponential, and then it becomes practically linear, due to the very high series resistance of the P-Si film.

Figure 5.10b shows the variation of current with temperature for porous silicon measured at low voltage.

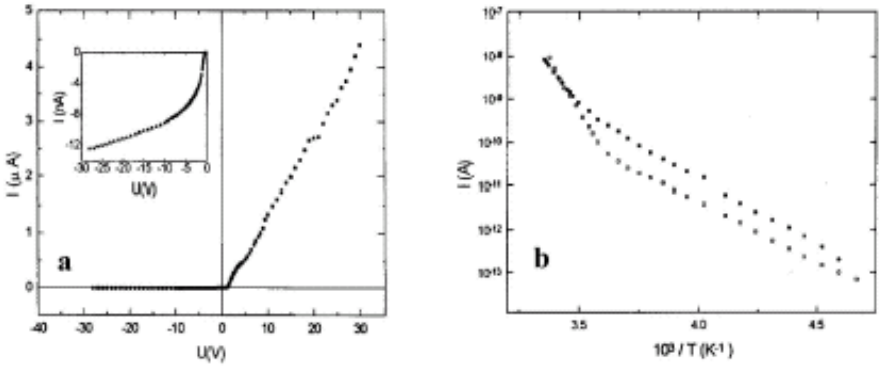

Figure 5.10a) I – V characteristic for oxidized PS samples at RT; b) I – T characteristic for Oxidized P-Si samples: ■ U_b = 2 V ('+' on c-Si), □ U_b = -2 V [24].

5. 3. 5 Optical Properties and Absorption

The dimension of the p-Si structures (i.e., the pore size and the porous layer thickness), compared to the optical wavelengths λ, can range from $l << \lambda$ all the way to $1 \approx \lambda$. There are accordingly two different regimes of light propagation and interaction with p-Si.

The *first regime* is $l << \lambda$ The radiation fields cannot resolve the P-Si structures, and the interaction can be conveniently described by means of an *effective medium approximation*, where a macroscopic dielectric constant (or a refractive index) is evaluated as a suitable combination of the dielectric constants of Si and air. The result is in general a complex dielectric function of space.

The *second regime* is $l \approx \lambda$; these kinds of structures are called *mesoscopic*: the structural size is small compared to the wave coherence length — i.e. the maximum lengths along which phase memory and coherent phenomena are observable. The porous geometrical structure strongly influences light transport and interaction.

Mixed regimes are also possible in p-Si. The most important case is one-dimensional (1D) mesoscopic structures: the anodization parameters are set to achieve micro porous P-Si, (size of pores $<<\lambda$, first regime), but the anodizing current density is modulated to obtain periodical or a periodical thin layer structures (thickness $\approx \lambda$, second regime along the P-Si growth direction). Each layer is different from adjacent layers in terms of porosity and thus of effective dielectric constant (and effective refractive index). Compared to other thin-film growth techniques, p-Si has the advantage of allowing a *continuous* tuning of the refractive index over a wide range ($1.4 \leq n_{eff} \leq 2.4$), and of being a fast and cheap technique that can lead to structures of several *hundreds* of layers, with typical fabrication times ranging from few minutes to few hours.

The absorption coefficient has been measured in p-Si by optical transmission, photoluminescence excitation (PLE), and photo thermal deflection spectroscopy (PDL). Transmission spectra are shifted towards higher energy compared to bulk Si with a shift, which increases with increasing porosity. This observation is consistent with quantum confinement model.

The line shape analysis of the absorption coefficient shows that its energy dependence follows a trend like that of an indirect gap semiconductor similar to Si, but displaced to higher energy.

A characteristic feature of p-Si is the large displacement (Stokes-shift) between the absorption edge and the emission peak energy as indicated in Figure5.11. The existence of localized states that can account for the observed shift has been demonstrated. Such states can lead to self-trapped excitons at some surface bonds of Si crystallites, such as Si-Si dimers and Si-O double bonds, giving reduced dependence of the luminescence energy on size, and a very large Stokes shift. Other models for the Stokes-shift are based on Si quantum dot relaxation from distorted configurations, giving rise to new transitions involving localized states that lower the emission threshold with respect to the absorption.

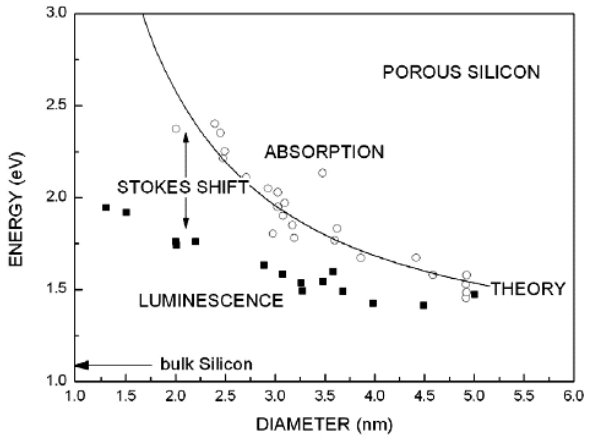

Figure 5.11. Compilation of optical band gaps of P-Si samples obtained from optical absorption (Un-filled symbols) and luminescence (filled symbols). The lines represent calculated values.

Limitations of Porous Silicon

Devices based on porous silicon exhibit room temperature EL spectra in the visible range. However, Porous silicon has a series of disadvantages .The main striking ones are:

- Poor stability due to the high porosity and

-The difficulty of integration of the electrochemical etching needed to produce porous silicon with the silicon VLSI technology [8].

UNIT-SIX

6. Silicon Nanocrystals (Si-ncs)

A nanocrystal is a single crystal having diameter of a few nanometers. Silicon/silicon dioxide, (Si/SiO_2) nanocrystalline quantum dots are silicon clusters, completely embedded in silicon dioxide [23]. The Si nanocrystals in the Si-related nanoparticles are ideal quantum dots with a stable surface, where carriers (electrons and holes) and phonons are to be confined [24]. The physical properties unique to silicon quantum dots make Si more attractive as a material of optoelectronic and functional devices. The sizes of Si quantum dots can be precisely controlled by their interaction with coherent light causing so-called photo-oxidation. In this chapter we discuss the different properties of silicon nanocrystals and their different synthesis methods. Figure6.1 shows silicon nanocrystals embedded in silicon dioxide.

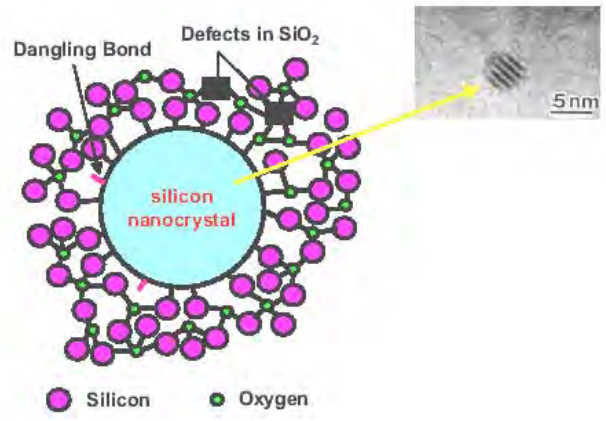

Figure 6.1Silicon nanocrystals embedded in SiO_2

6.1 Synthesis of Silicon Nanocrystals

Since necked silicon clusters are highly reactive they are mostly synthesized in a molecular beam under high vacuum condition [25]. Present silicon nanocrystals research is focused on the preparation of silicon nanocrystals embedded in an oxide host. With regard to a strong photoluminescence of the nanocrystal silicon in the visible spectra range the control of size, passivation and density is mandatory [26]. A blue shift of the luminescence is observed with decreasing nanocrystal size. The size control is realized by changing the chemical stoichiometry of the films. Reduction of the implanted silicon dose or the oxygen enrichment is the usual way for a decrease in nanocrystal size. Silicon nanocrystals

embedded in $Si0_2$ can be obtained by using several preparation techniques, such as laser ablation, aerosol technique, sputter decomposition, ion implantation, chemical vapor decomposition (CVD) or plasma enhanced chemical vapor decomposition (PECVD) [8].

These techniques can be divided into three main approaches: direct synthesis of silicon clusters, formation of a silicon reach layer and subsequent thermal induced phase separation and electrochemical erosion of bulk silicon [14]. Figure 6.2 gives schematics of these techniques

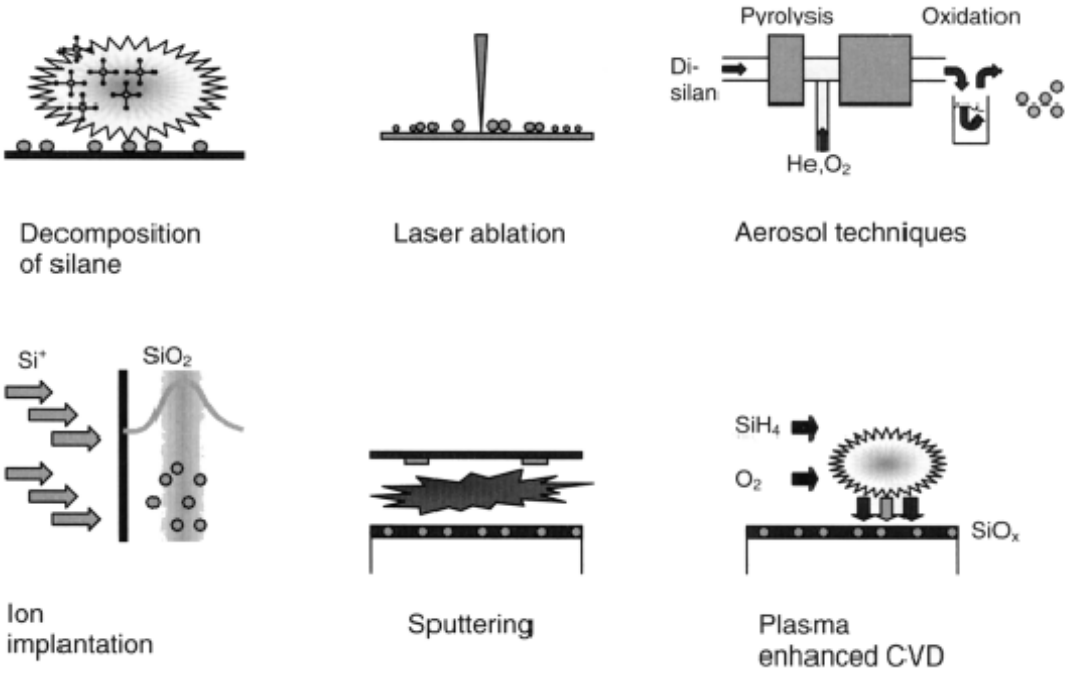

Figure 6.2 silicon nanocrystal fabrication techniques.

- *Laser ablation*: - in this method the silicon surface is evaporated by an energetic laser flux and Si-nc are formed by condensation in a gas cell, whose pressure controls, along with the power of the laser pulse the dimensions of Si-nc.
- *Aerosol technique*: - Here Si-nc are formed and dispersed in a carrier gas flow where they may undergo oxidation processes or also size selection by precipitation.
- *Sputtering decomposition*: - Ar^+ ions are used to hit a target made of Si and SiO_2. The silicon and oxygen atoms so obtained are then deposited on a substrate in order to obtain SiOx films, from where Si-nc are obtained by a subsequent thermal annealing.

- *Ion-implantation*: - Si-nc can be produced by implanting silicon ions at high doses into silicon dioxide film, followed by high temperature annealing to induce precipitation and form the Si-nc as illustrated in figure 6.3.

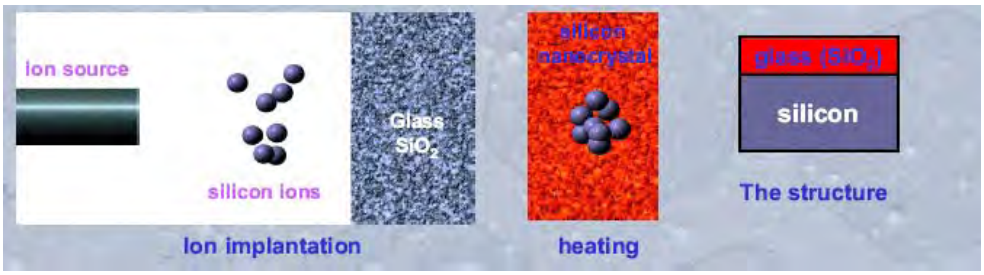

Figure 6.3 Synthesis of Si by ion implantation method.

- *PECVD technique*: - this technique is fully compatible with the Si VLSI technology and recently it has been shown that PECVD of sub-stoichiometric silicon oxide (SiO_x) layers followed by high temperature annealing represents a quite powerful method to produce Si-nc embedded with in SiO_2.

PECVD allows the deposition of thin films by using an electric discharge to induce chemical reactions in a gas. The plasma is generated by the application of an rf field to a low pressure gas, thereby creating free electrons within the discharge region. The reactive species generated by the plasma are then adsorbed on the substrate surface, where they are subjected to ion and electron bombardment, rearrangements, reactions with other adsorbed species, new bond formations, leading to film formation and growth.

The deposition process is dependent on the control and optimization of several deposition parameters including rf power density and frequency. Another important parameter in PECVD is the design of the reactor and the electrode configuration. RF tuning networks of PECVD systems usually employ an inductor, which shunts the powered electrode to establish this condition. Figure 7.4a gives the schematic of the apparatus for Si-nc synthesis. It is a PECVD system, consisting of an ultra high vacuum chamber, a load-lock, and 4-gas lines equipped with mass flow meters. An rf generator is connected through a matching network to the top electrode of the reactor; the bottom electrode is grounded and acts also as sample holder. In the bottom electrode, there are lamps to heat the substrate.

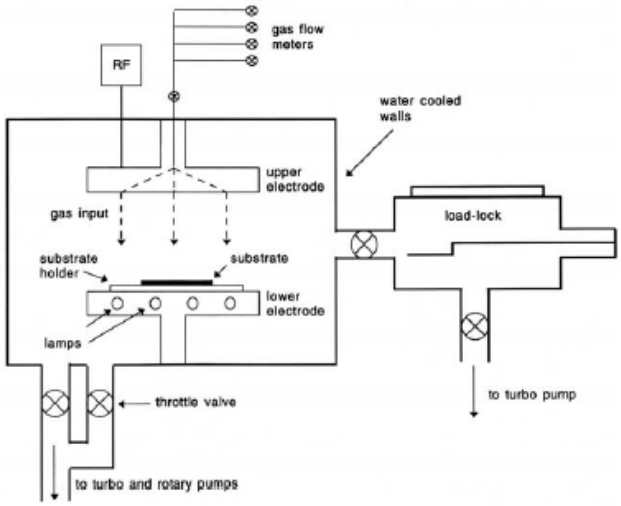

Figure 6.4a) Scheme of the PECVD apparatus used for the deposition process

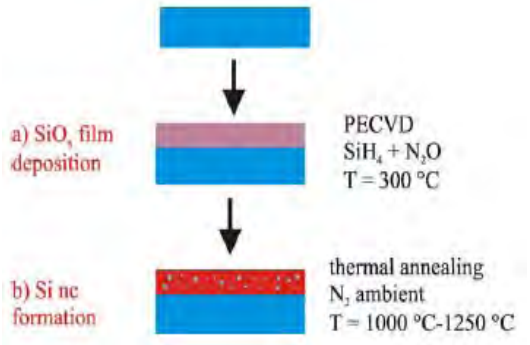

Figure6.4b) Steps for the preparation of Si

Figure6.4b) shows the steps for the preparation of Si-nc. The first step is the deposition by PECVD of sub-stoichiometric SiO_x with $x<2$ on a silicon wafer, by using SiH_4 and N_2O gaseous precursors and input power. After deposition, the films were annealed at high temperature to induce the separation of the SiO_2 and Si phases from the initial homogeneous SiOx phase and formation of Si-ncs embedded in silicon oxide The annealing process leads to the formation of Si-ncs, but also to the elimination of the hydrogen because the bonds Si-H are weak and therefore it is possible to break them easily. On the other hand, the Si-N bonds are stable and hence N is not eliminated by the annealing process but it remains embedded in the matrix.

In ion-implantation, plasma or low pressure CVD and sputtering techniques, Si-nc is formed by phase separation [14]. The difference among them is related to the degree of purity of the film (better for ion implanted samples), to the degree of defect incorporated to the porosity of the deposited films (greater for sputtered samples), to the control of the Si-nc content profile (better for the CVD films).

After deposition, the films are thermally treated at high temperature to induce the phase separation between silicon and the dielectrics. If SiO_2 is used as a dielectric, typical temperatures for the formation of Si-nc are between 900-1200^{o}c

6.2 **Characterization of Silicon Nanocrystals**

Once a sample is synthesized characterization of the size and morphology of the synthesized material is analyzed using AFM, diffraction methods, Raman spectroscopy and surface reactivity method.

Silicon nanoparticles formed as deposits or composite materials typically show nearly spherical geometrically in high-resolution transmission electron spectroscopy.

In the synthesis of silicon nano crystals by thermal vaporization of silicon in argon buffer gas followed by exposure to atomic hydrogen to passivate the surface on highly oriented graphite (HOPG) substrate. X-ray diffraction and high-resolution transmission electron microscopy (HRTEM) on these samples verify that nc-Si is indeed crystalline and approximately spherical (Figure6.5a) [27]. The distribution in the diameter of the Si-nc is determined from the z-scale of the AFM image (figure 6.5b)

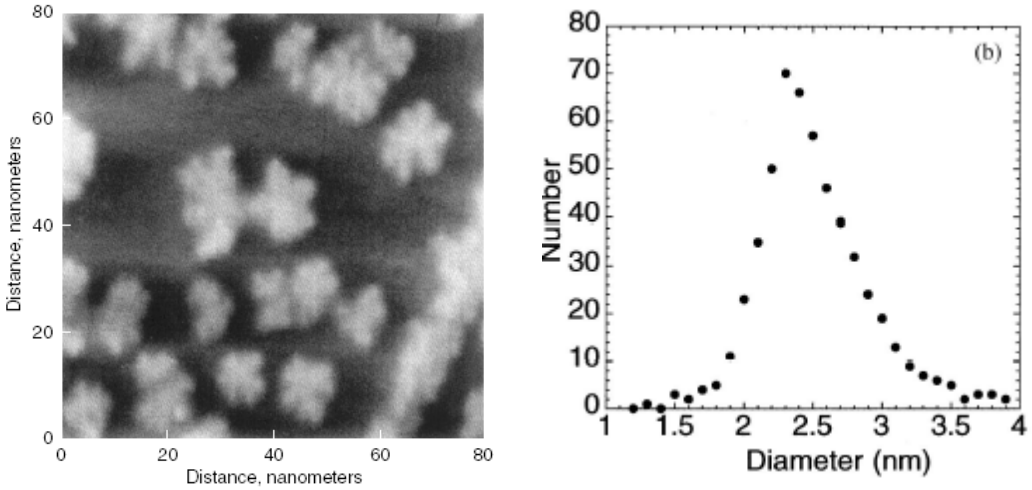

Figure 6.5(a) AFM image of Si-nc on the basal plane of HOPG formed by evaporation of at $1700^{0}c$ in argon buffer gas. (b) The size distribution of the Si-nc determined from the AFM height mode

Si-nc fabrications by the precipitation of excess Si in silicon rich oxides (produced by PECVD) produce nanocrystals with mean diameters in the range of 3-5nm.The resulting HRTEM micrograph of Si-nc in SiO_2 and the corresponding size distributions are shown in Figure 6.6a and b.

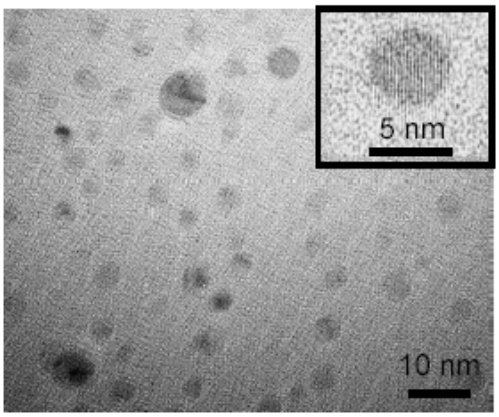

a)

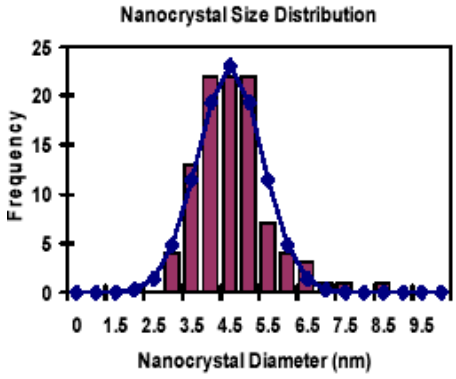

b)

Figure 6.6a) HRTEM micrograph of Si-nc in SiO2.Implant condition; 100KeV Si-; corresponding to an excess Si conc. of 10at. % at projected range of150nm Annealed 1100c; 16hr b) Size distribution of Si-nc.

6.3 Properties of Silicon Nanocrystals

6.3.1 Optical Properties of Silicon Nanostructure

In the early 1990s, there was a new development for nonstructural silicon. Bulk silicon, when electrochemically etched was made porous and was found to show photoluminescence in the visible range. Soon the new effect was attributed to silicon nanowires or particles present in the structure [11]. In deed, scanning tunneling microscope (STM) studies of the porous silicon surface show the presence of nanoparticles. It was supposed by the observation that individual silicon particles showed photoluminescence.

Quantum confinement effects are prominent in porous silicon, which has led to a wide range of studies into its opto-electronics properties.

The origin of visible photoluminescence (PL) from nanoscale Si is still the subject of much debate. Views are polarized between quantum confinement and other mechanisms. An explanation based on quantum size effects alone does not explain all observation. Surface species, surface states, fabrication wavelength and pore structure also play a role [11]. Efficient emission of visible light has been observed from the nanostructure of silicon when it is exposed to ultra violet light.

The indirect band gap silicon causes a very long radiative lifetime (ms) for excited electron-hole pairs. Competing non-radiative recombinations also prevail and cause most of

the excited electron-hole pairs to recombine non-radiatively. This yields very low internal quantum efficiency ($\eta \approx 10^{-6}$) for Si luminescence [27].

The production of red light in silicon dot results from the electron-hole pair recombination across the band. The quantum confinement effect changes the energy level continuum in the bulk material into a discrete level structure namely the sub-band structure. This leads to the enhancement of the oscillator strength of the exciton through increased spatial overlap between the electron and the hole. The dielectric confinement also enhances the exciton binding energy and the exciton oscillator strength for dots having size of the order of exciton Bohr radius.

It has been surmised that nanostructures of silicon have a direct band gap and emit light from violet to red depending up on the size of the structures [28]. With a large surface-volume ratio, the surface effects become more enhanced. Therefore, geometry plays an important role. Surface effects as well as quantum confinement effects control the optical and electrical properties of these materials.

Behind the hope to increase the radiative recombination rate by exploiting quantum confinement in silicon nanocrystals, another effect improved the emission efficiency of Si-nc. This is the spatial localization of excited electron hole in a small region of the sample. Electron-hole pairs are locally excited: if the nanocrystal is free of recombination centers (killer center) the electron and holes recombine radiatively. In this case, the nanocrystal is bright. If the nanocrystal has a recombination center, the electron and hole recombine non-radiatively and thus the nanocrystal is dark [14]. Figure 6.7 shows a system of three electron-hole pairs of internal quantum efficiency 2/3 (~67%).

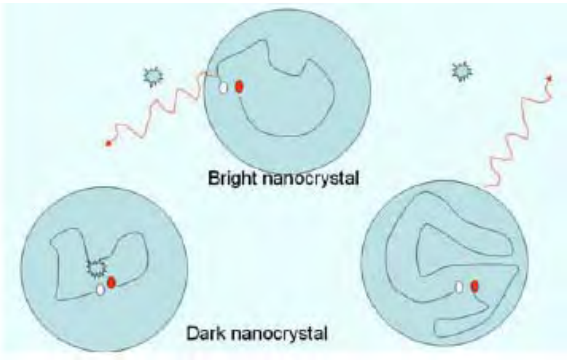

Figure 6.7 Three electron–hole pairs are locally excited of which one recombines non-radiatively and two radiatively

Recent photoluminescence experiments have shown a structural emission spectrum, which is interpreted in terms of crystalline silicon phonon assisted recombination.

Si-ncs show an intense light emission at room temperature in the inner infrared or in the visible region. In fact amorphous SiO_x films have only weak light emission in the range 600-650nm; after the annealing process, when the Si-nc were formed the photoluminescence (PL) spectra evolve, giving as a result an intense light emission [8].

In an experiment, nanocrystalline Si particles fabricated by pulsed plasma processing technique show infrared luminescence from the as grown film at room temperature [29].

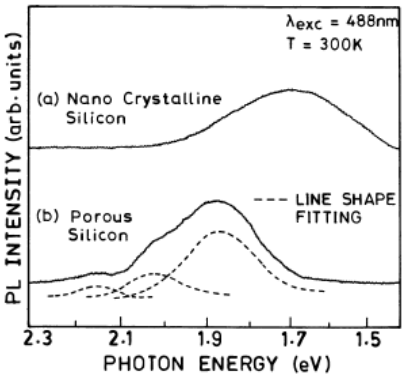

Figure 6.8 Room temperature Raman spectra of
a) Nc-Si prepared by pulsed plasma processing and
b) Porous Si prepared by anodic etching

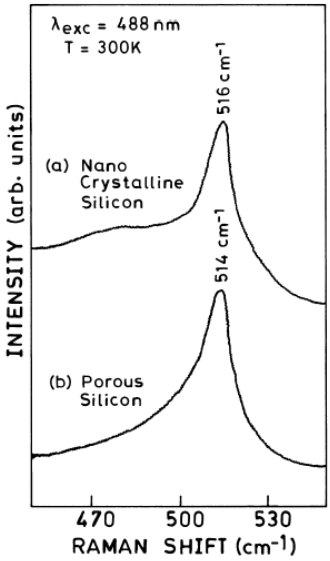

Figure 6.9 PL spectra of (a) nc-Si and (b) Porous Silicon

Raman spectra from these films consisted of broad band super imposed on a sharp line as indicated in figure 6.8.The sharp line, whose intensity, frequency, and width depend on the particle size, is expected to arise from the phonon confinement in nanometer sized crystalline silicon. The broad Raman band resembles that of the density of states spectrum in amorphous silicon and indicates the presence of amorphous silicon like structure in the film.

Photoluminescence measurements performed by pumping with a 488nm line of an Ar-Kr ion laser to measure room temperature spectra of SiO_x film having a known Si concentration for different annealing temperatures show that the wave length of the PL peak (λ_{max}) increase with the annealing temperature [8]. PL spectra measurements also show λ_{max} shift for different Si composition of SiO_x films annealed at a given temperature (fig. 6.10).

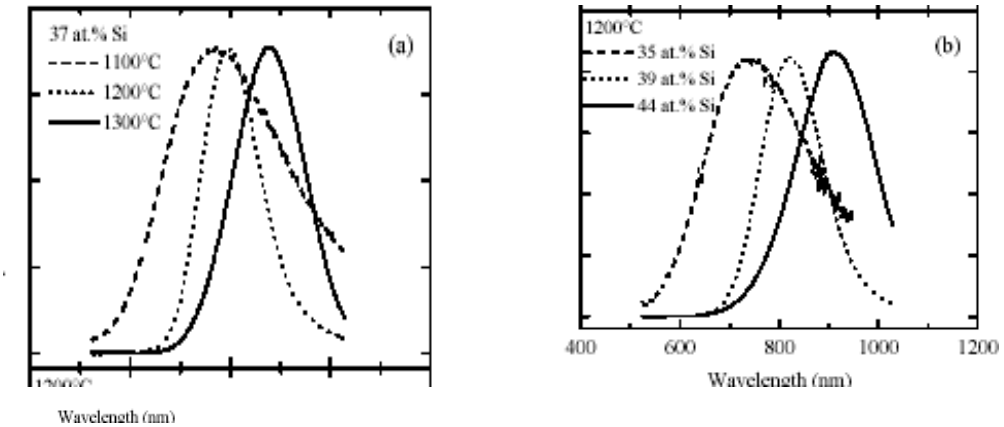

Figure 6.10 Normalized room temperature of (a) a SiOx film having a Si concentration of 38%after thermal annealing Process performed at 1100, 1200 and 1300 for 1hr. (b) SiOx films having Si concentration of 35, 39 and 44 after a thermal annealing process at 1200^0c for 1hr.

6.3 2 Energy Band Shift

It is generally agreed that quantum confinement caused by the restricted size of the nanometer scale silicon particles is essential for the light emitting properties. A prediction of the quantum confinement model is that the energies of the valence band (VB) and conduction band (CB) edges are shifted relative to the bands of bulk silicon, leading to an increased energy gap. This is confirmed from the comparison of the band edge spectra of the nanocrystal with that of the bulk. Figure 6.11a) illustrates the absorption spectra for bulk and nanocrystalline silicon.

According to the quantum confinement theory, electrons in the conduction band and holes in the valence band are confined spatially by the potential barrier of the surface or trapped by the potential well of the quantum box. Because of the confinement of both the electrons and holes, the lowest energy optical transition from the valence to the conduction band increases in energy, effectively increasing the energy gap (E_G). The sum of the kinetic and potential energy of the freely moving carriers is responsible for the E_G expansion and therefore, the width of the confined E_G grows as the characteristic dimensions of the crystallite decreases.

Recent bulk sensitive and element specific soft X-ray fluorescence measurements of the VB of silicon nano clusters also show a shift in the VB maximum that is comparable to the photoemission result [30]. This confirms that the photoemission measurement is measuring the true silicon valence band shift, not just a surface state or surface species.

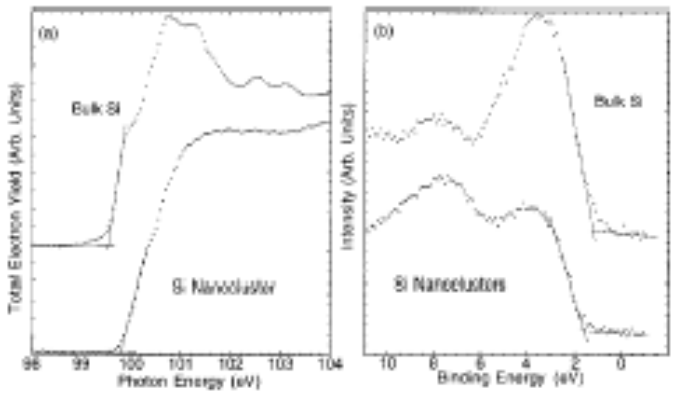

Figure 6.11 a) L2, 3 absorption spectra for bulk Si and nc-Si Deposited on oxidized Ge (d=1.6nm) b) Photoemission-spectra for the valence band of bulk silicon and the nc-Si (d=1.6nm), the VB referenced to the Si 2p core level.

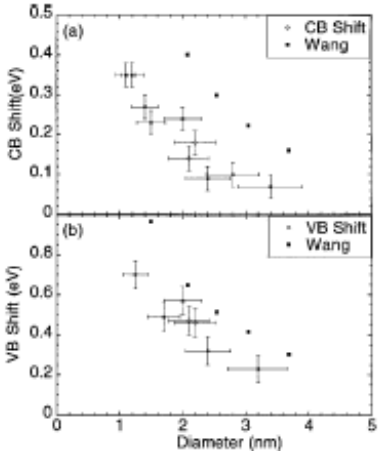

Figure 6.12a) The conduction band (CB) edge shift (b) the valence band (VB) edge shift as a function of nc –diameter. The solid squares represent the theoretical predicted edge shift for a H-terminated Si quantum dot VB & CB

If the observed VB and CB shifts are due to quantum confinement one would expect the size of the band shifts to increase as the particle size of the nanocrystalline Si is decreased. Figure 6.12a), and b) give the shift in the conduction band edge and the shift in the valence band edge for silicon nano cluster samples with different average sizes.

The band gap of the nano clusters as a function of the measured diameter, and comparison is made with PL and extended X-Ray absorption data from oxygen terminated silicon nano clusters and with theoretical results for spherical silicon clusters terminated with hydrogen. The VB and CB shifts subsequently result in the widening of the energy gap as a function of particle size as shown in figure 6.13.

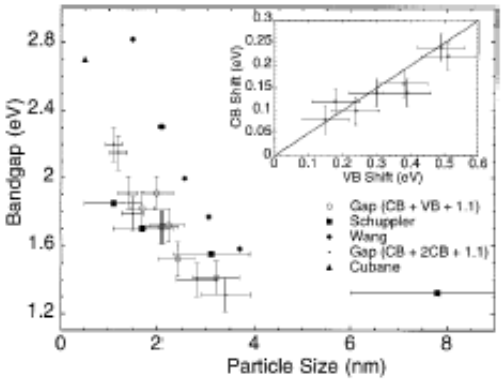

Figure 6.13 Band gap of the nc –Si a function of particle size.

Chemical bonds among the surface Si-atoms of the Si-nc and the atoms of the host strongly modify the energy spectrum of Si-nc [14].

6.3.3 Electrical Properties

The electrical transport properties of Si-nc are determined mainly by its microstructures. With silicon nanocrystals embedded in ultra thin oxide by the rapid thermal oxidation (RTO) of an ultra thin chemical vapor deposition (CVD) amorphous Si (a-Si: H) film, some novel features such as the current peak and valley and the hystersis are revealed in I-V characteristics curve of the diode structure. This suggests the charging of a definite amount of electrons at the silicon nanocrystals and the subsequent screening effect on the tunnel current following the diode structure [31].

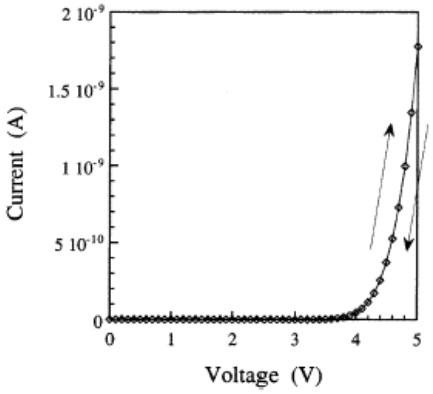

Figure 6.14 Typical static I–*V* characteristics of a 10 min-RTO diode sample (initial a–Si: H thickness of 10 nm) measured at room temp. where the measurements delay time is 60 s.

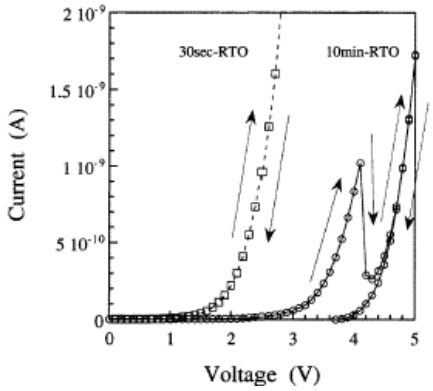

Figure 6.15 Typical dynamic *I–V* characteristics of 10 min (solid curve) and 30 s (dashed curve) RTO diode sample (initial a–Si: H thickness of 10 nm) measured at room temp., where the measurement Delay time is 0 s.

Figure 6.14 shows the typical round sweep I-V characteristics of a 10-min –RTO diode sample where the delay time is 60 second. The round sweep I-V characteristics measured under the delay time of 0 second for the same sample in figure7.14 is represented in figure 6.15. It should be noted that the I-V characteristics measured under the minimum delay time reveal the novel features of the current peak and valley at the gate voltage from 2.5-4.2V.in the forward sweep. In contrast, the reverse sweep I-V curve shows no current peak and valley in the forward sweeps is not attributed to the resonant tunneling. It is important to note that the formation of Si -ncs of less than 5nm in size leads to these novel features.

The time dependence of the tunnel current for the 10 min-RTO diode samples is summarized in figure 6.16.The experimental results in figures.7.15 and 7.16 can be

attributed to the electron charging related to the silicon nanocrystals and the consequent effect on the tunnel current .The exact electron trapping sites at the silicon nanocrystals are unknown at present. However, it is not considered that the electron stays in the conduction band of the silicon nanocrystal.

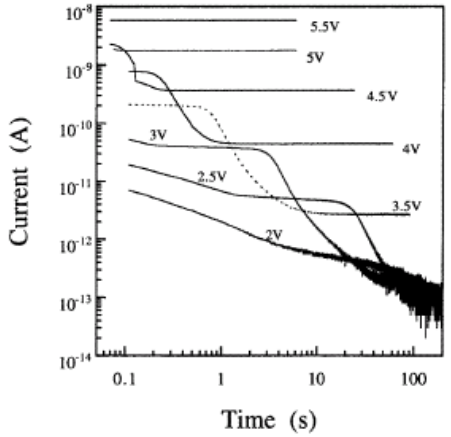

Figure6.16 Time dependence of the tunnel current (100 ms to 100 s) for the 10 min-RTO diode sample with the gate voltage as a parameter. The measurement was performed at room temperature.

6.3.4 Non-linear Optical Properties

In typical semiconductor nanocrystals, energy level spacing is in the order of about 0.2eV, depending on the material and quantum number. If the integrated oscillator strength over a range of 0.2eV compressed into line widths of a few meV, then applicability for non-linear optical devices and applications become a reality [2].

Non-linear optical properties are of major interest for photonic device applications such as all optical switching. Intensity dependent changes in the optical properties are prominent at high intensity (I) of pump laser, particularly third order nonlinear effects. Enhanced optical non-linearity has been reported for porous silicon at different wavelengths. Third order nonlinear effects are generally characterized by non-linear absorption (β) and non-linear refractive index (n_2). These are described by:

$$\alpha(I) = \alpha_o + \beta I \quad \text{..... (12)}$$

and $$n(I) = n_o + n_2(I) \quad \text{..... ..... (13)}$$

Where α_0 and n_o stands for linear absorption and refractive index, respectively. The β and n_2 values are used to evaluate the imaginary (I_m X $^{(3)}$) parts of the third order nonlinear

susceptibility. The most versatile technique to measure $I_m X^{(3)}$ and $R_e X^{(3)}$ is the single beam technique, referred as z-scan.

The real part of the third-order nonlinear susceptibility is obtained from

$$R_e X^{(3)} = 2n_o^2 \varepsilon_o c n_2 \quad \text{..... (14)}$$

Where ε_o is the permittivity of free space, c is velocity of light and n_o is the effective refractive index.

The non-linear absorption arises from either direct multi photon absorption or saturation of single photon absorption. By comparing $R_e X^{(3)}$ and Im $X^{(3),}$ one can conclude that $R_e X^{(3)} >> \text{Im}X^{(3)}$ i.e. the non-linearity is mostly refractive. The absolute values of $X^{(3)} = \left[(R_E X^{(3)})^2 + (\text{Im}\, X^{(3)})^2\right]^{1/2}$ are significantly larger than the bulk Si values and are of the same orders of magnitude as those reported for p-Si.

Due to quantum confinement it is found that the increase in the oscillator strengths caused by the confinement-induced localization of excitons originates the increase of $X^{(3)}$ [32]. Figure 6.17 shows the dependence on Si-nc radius r. The scatters could be attributed to effective refractive index and volume fraction of Si-nc in the embedded matrix.

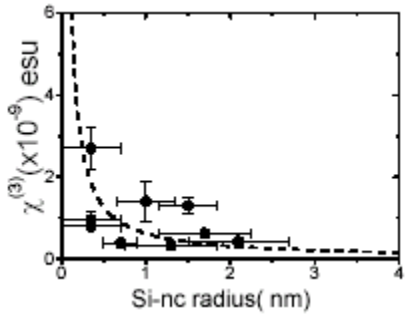

Figure 6.17 Variation of χ (3) with Si-nc radius (r) in Si-nc grown by PECVD. Inset shows the PL peak maxima variation with Si-nc radius. Dashed lines are a theoretical

The increase in $X^{(3)}$ follows more closely;

$$X_{si-nc}^{(3)} = X_{bulk}^{(3)} + \frac{A}{r} + \frac{B}{r^2} \quad \text{..... (15)}$$

In reality the experimentally determined $X^{(3)}$ is related to the microscopic $X_m^{(3)}$ by

$$X^{(3)} = P / f /^4 X_m^{(3)} \quad \text{..... (16)}$$

Where p is the volume fraction and f is a local field correction that depends on the dielectric constant of embedded matrix and nano crystal.

In a macroscopic crystal of silicon, one has about 10^{23} electrons and nuclei. In principle the application of the known laws of quantum mechanics allows one to predict all the physical and chemical properties of such a system. However, given the astronomical number of particles, it is absolutely hopeless to extract physically meaningful results with out some dramatic approximations. The pseudo-potential–DFT is one of these approximation methods the application of which is treated in the next chapter.

UNIT-SEVEN

7. The Pseudo-Potential-Density Functional Theory Applied to Nanostructures

The pseudo-potential model of a solid has led the way in providing a workable model and modern computers have provided the computational resource to allow the implementation of this method. For example, it is now possible to predict accurately the properties of complex systems such as quantum dots or semiconductor liquids with hundreds, if not thousands of atoms. These first principles pseudo-potentials often relay on density functional theories, which are exact in principle but in practice relay on various approximations such as the local density approximation [33]. The purpose of this chapter is to preview how to implement this approximation method in nanostructures such as that of silicon.

A solution to the electronic structure is obtained in this approach from the Kohn-Sham equation. The Kohn-Sham problem, cast with in the pseudo-potential–density functional formalism is easy to solve for simple elemental crystals such as silicon [34].

The pseudo-potential model treats matter as a sea of valence electrons moving in a background of ion cores (fig.7.1). The cores are composed of nuclei and inert inner electrons. The ion cores composed of the nuclei and tightly bound core electrons are treated as chemically inert. The pseudo-potential model describes only the outer, chemically active, valence electrons

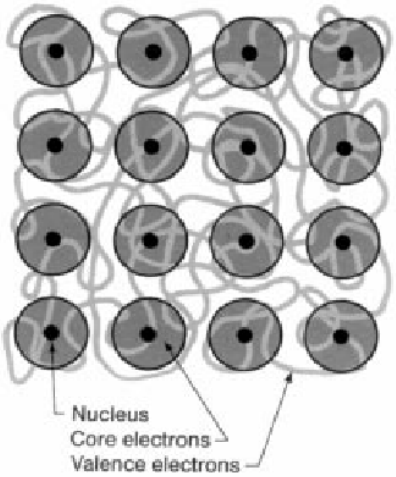

Figure 7.1 Standard pseudo-potential of a solid.

7.1 Constructing Pseudo-potentials

Most pseudo-potential are almost always based on density functional theory (DFT). Within DFT, the many body problem is mapped on to a one-electron Hamiltonian. The effect

of the exchange and correlation interactions is subsumed into a one electron potential that depends on the charge density.

This mapping of the many body problems to a one-body problem often incorporates an additional approximation- the local density approximation (LDA). LDA allows one to construct self-consistent field pseudo-potentials for condensed matter systems. The chief limitation of these approximations is that they are appropriate only for the ground state structure and cannot be used to describe excited states without other approximations. As such one uses LDA to determine structural energies, compressibility elastic constants, vibration modes and so on, but not band gap from the eigenvalue spectra [34]. With respect to band gap and electronic excitations, it is possible to consider these by implementing linear response theory on top of standard LDA calculation.

According to the Kohn and Sham approach, for an isolated atom, one can write down a one-electron Hamiltonian and the corresponding one-electron Schrödinger equation using LDA:

$$\left\{ \frac{-\hbar^2\nabla^2}{2m} - \frac{Ze^2}{r} + V_H(r) + V_{xc}[r,\rho(r)] \right\}\psi_n(r) = E_n\psi_n(r) \ldots\ldots\ldots\ldots \quad (17)$$

Where there are Z-electrons in an atom, V_H is the Hartree potential, and V_{xc} is exchange correlation potentials; V_H and V_{xc} can be determined from the electronic charge density [35]. The eigenvalue and the eigenfunctions; E_n and $\psi_n(r)$ respectively can be used to determine the total electronic energy of the atoms.

The density is given by:

$$\rho(r) = -e\sum_{n,occup}|\psi_n(r)|^2 \ldots\ldots\ldots\ldots \quad (18)$$

V_H is then determined by:

$$\nabla^2 V_H(r) = -4\pi e\rho(r) \ldots\ldots\ldots\ldots \quad (19)$$

This term can be interpreted as the electrostatic interaction of the electron with the charge density of the system.

With the DFT, one can define V_{xc} as a function of the charge density. The central tenant of the LDA is that the total exchange correlation energy may be written as:

$$E_{xc}[\rho] = \int \rho(r)E_{xc}\rho(r)d^3r \ldots\ldots\ldots\ldots \quad (20)$$

Where E_{XC} is the exchange correlation energy density; with knowledge of E_{xc}, one can extract the potential and the total electronic energy of the system.

It is a common practice to separate exchange and correlation contributions. i.e.,

$$E_{xc} = Ex + E_c. \quad \text{(21)}$$

It is also convenient to define an electron gas parameter, r_s where r_s is given by;

$$r_s = \left(\frac{3}{4\pi\rho(r)} \right)^{1/3} \quad \text{(22)}$$

A simple form of E_x can be obtained by evaluating the potential for a homogeneous electron gas:

$$E_x(r_s) = \frac{0.4582}{r_s} \quad \text{(23)}$$

For the correction contribution (E_c) to this potential, different forms have been proposed. One of the most popular arises from Monte Carlo simulation on free electron- gas. The results from the simulation are numerically parameterized for convenient implementation.

One commonly used form is:

$$E_c(r_s) = -\frac{0.1432}{1+1.0529\sqrt{r_s}+0.334r_s} \quad \text{for } r_s \geq 1 \quad \text{(24)}$$

and $E_c(r_s) = -0.0480 + 0.0311\ln r_s - 0.0116 r_s \, 0.0020 r_s \ln r_s$ for $r_s < 1$ (25)

Once E_{XC} is known, the potential energy can be obtained from the functional derivatives:

$$V_{xc}[r, \rho(r)] = \frac{\partial E_{xc}[r_s]}{\partial r_s} \frac{\partial r_s}{\partial \rho} \quad \text{(26)}$$

This potential can be explicitly written as;

$$V_{xc}[r, r_s] = E_{xc}[r, r_s] - \frac{r_s}{3}\left(\frac{dE_{xc}}{dr_s} \right) \quad \text{(27)}$$

It is not difficult to solve Eq. (17), the Kohn-Sham equation, for an atom. The charge density is taken to be spherically symmetric. Thus, the problem reduces to solving a one-dimensional problem. V_H and V_{xc} can be iterated to form a self-consistent field. Kerker proposed a straightforward method for constructing a local density pseudo-potential that retained the norm-conserving criterion. He suggested that the pseudo wavefunction has the form:

$$\phi_p(r) = r^l \exp p(r) \qquad \text{for } r< r_c. \text{ ……………………………………. (28)}$$

Where $P(r) = -ar^4 - a_1r^3 - a_2 r^2 - a_3$ is a polynomial and

$$\phi_p(r) = \psi_{AE}(r) \qquad \text{for } r > r_c \text{ ………………………………………………. ….(29)}$$

While all local density pseudo-potentials impose the condition that

$\phi_p(r) = \psi_{AE}(r)$ for $r > r_c$ the construction for $r < r_c$ is not unique.

One straightforward approach to optimize pseudo-potential is to build additional constraints into the polynomial given in Eq.28. For example, suppose we write

$$p(r) = c_0 + \sum_{n=1}^{N} c_n r^n \qquad \text{(in Kerker's scheme N=4)……………………..… (30)}$$

Once the pseudo-wavefunction is defined as in Eqs. (28) and (29), we can invert the Kohn-Sham equation and solve for the ion core pseudo-potential, Vion, p.

Since the ion cores can be treated as chemically inert and highly localized, it can be written as:

$$V_{ion}(r) = \sum_{R_a} V_{ion,a}(r - R_a) \text{ …………………………………………………... (31)}$$

Where $V_{ion,\, a}$ is the ion pseudo-potential associated with the atom, a, at a position R_a.

This potential, when self consistently screened by the pseudo charge density;

$\rho(r) = -e\sum \left|\phi_{p,n}(r)\right|^2$ will yield an eigenvalue of E_n and a pseudo-wave function $\phi_{p,n}$. The pseudo-wavefunction by construction will agree with all the electron's wave functions away from the core. With the eigenvalue problem solved, the total energy of the system, E_{tot}, can be evaluated from;

$$E_{tot} = \sum_{occup} E_n - \frac{1}{2}\int d^3r\rho(r)V_H(r) + \int d^3r\rho(r)E_{xc}[r,\rho(r)] - V_{xc}[r,\rho(r)] + E_{i-i}[R_a] \text{ …..... (32)}$$

Where $E_{i\text{-}i}$ is the ion–ion repulsion.

If one knows the behavior of the total energy as a function of atomic position, it is possible to compute inter atomic forces and perform *ab initio* molecular dynamics. Since the pseudo-potential is weak, simple basis sets such as a plane wave basis can be quite effective for crystalline matter. For example, in the case of crystalline silicon only 50-100 plane waves need to be used. The resulting matrix representation of the Schrödinger operator is dense in Fourier (plane wave) space. The matrix vector product operations are performed

with the help of fast Fourier transforms (FFT). The plane wave method uses a basis of the form;

$$\psi_k(r) = \sum_G \alpha(K,G)\exp(i(K+G))\cdot r \quad (33)$$

Where K is the wave vector, G is a reciprocal lattice vector and $\alpha(K,G)$ represents the coefficients of the basis.

An alternative approach is to avoid the use of a basis .For instance; one can use a real space method that avoids the use of a plane wave and FFTs altogether. Here a particular version of this approach called the finite-difference pseudo-potential method is illustrated. This approach utilizes finite difference discretization on a real space grid. If a uniform grid is imposed on a system where the points are described in a finite domain by (x_i, y_j ,z_k) we approximate $\frac{\partial^2\psi}{\partial x^2}$ at (x_i, y_j, z_k) by ;

$$\frac{\partial^2\psi}{\partial x^2} = \sum c_n\psi(x_i + nh, y_j, z_k) + o(h^{2M+2}) \quad (34)$$

Where h is the grid spacing and M is a positive integer. This approximation is accurate to o (h^{2M+2}) upon the assumption that ψ can be approximated accurately by a power series in h.

With the kinetic energy operator expanded as in Equation (34) one can set up a one electron Schrödinger equation over a grid [33, 34, 35]. The wave function $\psi(x_i, y_j, z_k)$ is computed on the grid by solving the eigenvalue problem;

$$\frac{-h^2}{2m}\left\{\sum_{n1=-M}^{M} C_{n1}\psi_n(x_i + n_1h, y_j, z_k) + \sum_{n2=-M}^{M} C_{n2}\psi_n(x_i, y_j + n_2h, z_k) + \sum_{n3=-M}^{M} C_{n3}\psi_n(x_i, y_j, z_k + n_3h)\right\} +$$
$$\left[V_{ion}(x_i, y_j, z_k) + V_H(x_i, y_j, z_k) + V_{xc}(x_i, y_j, z_k)\right]\psi_n(x_i, y_j, z_k) = E_n\psi_n(x_i, y_j, z_k) \quad (35)$$

If we have L grid points, the size of the full matrix resulting from the problem is L X L. Each grid point corresponds to a row in the matrix. Fig.7.2 gives a uniform grid illustrating a typical configuration. However many points in the cube are far from any atom in the system and the wave function on these points may be set equal to zero. In the discrete form, the non-local term becomes a sum over all atoms, a, and quantum numbers (l, m) of rank one updates;

$$V_{ion} = \sum_a V_{loc,a}a + \sum_{a,l,m} C_{a,l,m}u_{a,l,m}u^T_{a,l,m} \quad (36)$$

Where $u_{a,\,l,\,m}$ are sparse vectors which are only non-zero in a localized region around each atom, and $C_{a,\,l,\,m}$ are normalization coefficients.

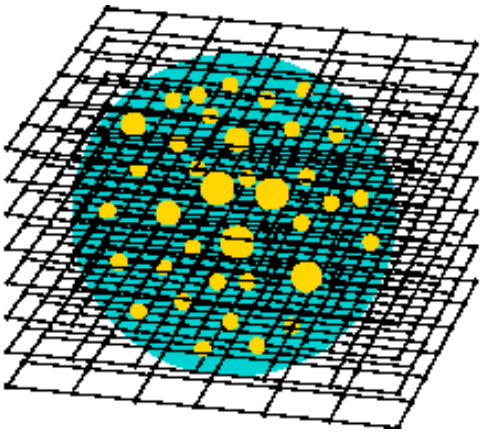

Figure 7.2 Uniform grids illustrating a typical configuration for examining the electron structure of a localized system. The gray sphere represents the domain where the wave functions are allowed to be non-zero. The light spheres within the domain are atoms

A popular form of extracting the eigen pairs is based on the generalized Davidson method in which the pre-conditioner is not restricted to be a diagonal matrix. Pre-conditioning technique in this approach are typically based on filtering ideas and the fact that the Laplacian is an elliptic operator. The eigenvectors corresponding to the few lowest eigenvalues of ∇^2 are smooth functions and so are the corresponding wave functions. When an approximate eigenvector is known at the points of the grid, a smoother eigenvector can be obtained by averaging the value at every point with the values of its neighboring points.

Methods based on approximation inverse techniques have been somewhat more successful, performing better than filtering at additional preprocessing and storage cost. However, filtering techniques are inexpensive to apply and result in substantial savings in iterations.

7.2 Structures of Silicon Nanocrystals–A Computational Approach

Nanocrystals possess properties that are characteristic of neither the atomic nor solid states. For example, the energy levels in atoms may be discrete and well separated in energy relative to KT. In contrast, solids have continuum of states (energy bands). Clusters may reside between these limits, i.e., the energy levels may be discrete, but with a separation much less that KT.

The most fundamental issue in dealing with nanocrystals is determining their structure. Before any accurate theoretical calculations can be performed for a cluster, the atomic geometry of a system must be defined.

Real space methods are easily suited for investigating these systems. Serious problems arise form the existence of multiple local minima in the potential energy surface of these systems; many similar structures can exist with vanishing small energy differences. A complicated issue is the transcriptions of inter atomic forces in to tractable classical force fields. This transcription is essentially difficult for clusters such as those involving semi-conducting species. In these clusters, strong many body forces can exist that preclude the use of pair wise forces.

A convenient method to determine the structure of small or moderate sized clusters is simulated annealing. With in this technique, atoms are randomly placed within a large cell and allowed to interact at a high (usually fictive) temperature.

Langevein molecular dynamics is well suited for simulated annealing methods. In Langein dynamics, the conic positions, Rj, evolve according to;

$$M_j \ddot{\vec{R}}_j = \vec{F}\left(R_j\right) - \gamma M_j \dot{\vec{R}}_j + G_j \quad \text{..... (37)}$$

Where $\vec{F}\left(R_j\right)$ is the inter-atomic force on the j-th particle, and M_j are the ionic masses. The last two terms on the right hand side of Eq. (37) are the dissipation and fluctuation forces, respectively [35]. The dissipative forces are defined by the friction coefficient, γ. The fluctuation forces are defined by random Gaussian variables, $\vec{G}_j$ with a white noise spectrum:

$$\left\langle G_i^{\alpha}(t)\right\rangle = 0 \quad \text{and} \quad \left\langle G_i^{\alpha}(t)\right\rangle\left\langle G_j^{\alpha}\left(t'\right)\right\rangle = 2\gamma M_j K_B T \delta_{ij}\delta\left(t-t'\right) \text{..... (38)}$$

The angular brackets denote ensemble or time averages, and α stands for the Cartesian component. The coefficient of T on the right hand side of Eq.38 insures that the fluctuation-dissipation theorem is obeyed, i.e., the work done on the system is dissipated by the viscous medium.

The inter atomic force, F_i^{α}, on an atom located at $\vec{R}_a$ in the α direction for a finite system is obtained using the Hellmann Feynman theorem;

$$F_a^{\alpha} = -\frac{dE_{tot}}{dR_a^{\alpha}} = -\frac{\partial E_{e-i}}{\partial R_a^{\alpha}} - \frac{\partial E_{i-i}}{\partial R_a^{\alpha}} \quad \ldots\ldots\ldots\ldots\ldots\ldots\ldots\ldots\ldots\ldots\ldots\ldots\ldots\ldots \quad (39)$$

Where E_{tot} is the total ground state energy.

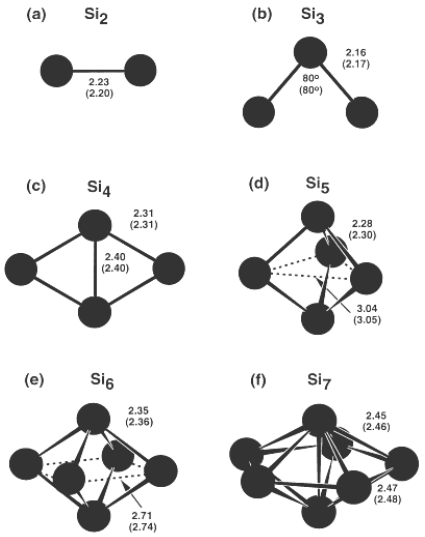

Figure 7.3 Ground state geometries and some low-energy isomers Si_n ($n \leq 7$) clusters.

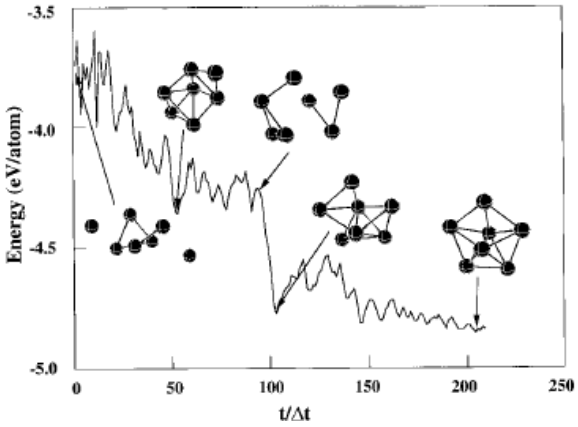

Figure 7.4 Binding energy of Si_7 during a Langevein simulation.

The inter-ionic core interaction is simply the point-charge interaction. Once the inter atomic forces are determined, it is straight for word to implement simulated annealing. An initial atomic configuration is chosen and the system is then heated to a high temperature. As the system is cooled, only lower energy structures form. If the anneal is done slowly, it is possible to achieve the ground state structure. Figure 7.4 gives the ground state structure of silicon cluster of seven atoms, which is obtained by simulated annealing procedure. Figure 7.3 presents the ground state structures for si_n for $n \leq 7$.

7.3 Modeling the Quantum Dot.

Silicon dots can be modeled by considering a bulk-terminated cluster of Si atoms caped off by H atoms (or H-like atoms) [37]. The dangling bonds are saturated with hydrogen like atoms. A ball and stick model of a silicon quantum dot is shown in figure 7.5

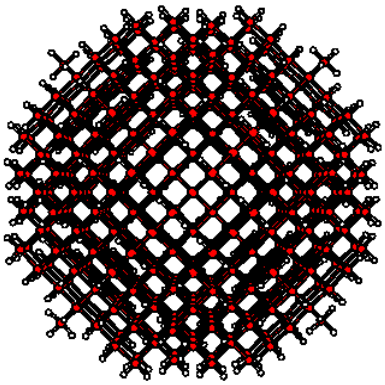

Figure 7.5 Atomic structure of a Si quantum dot with composition $Si_{525}H_{276}$

UNIT-EIGHT

8. Quasi-Particle Gap and Optical Gaps

8.1 Quasi-Particle Gaps in Quantum Dots

Excitations in confined systems, like silicon quantum dots as the building blocks of porous silicon, differ from those in extended systems due to quantum confinement. In particular, the compounds that comprise the excitation energies such as particle and excitation binding energies change significantly with the physical extent of the system.

Recent advances in electronic structure algorithms using pseudo-potential platforms and alternative formulations of the optical gaps suitable for confined systems enable to study quantum confinement-induced changes [35].This chapter is devoted to the discussion of these changes obtained computationally.

The quasi-particle gap, E_g^{qp}, is defined as the energy required to produce a non-interacting electron-hole pair [36]. For an n-electron system, the quasi particle gap E_g^{qp} can be expressed in terms of the ground state total energies E as:

$$E_g^{qp} = \left[E(n+1) - E(n)\right] + \left[E(n-1) - E(n)\right] \quad \text{..... (40)}$$

Where n is the number of electrons in the system. The first terms represents the energy to create an electron in the lowest empty state, the second term represents the energy to create a hole in the highest occupied state.

If one had the exact exchange-correlation functional the quasi particle energy would be accurately given by (40).

Within the local density approximation, in the limit of very large systems ($n \to \infty$), the quasi-particle gap approaches the gap between the highest occupied and the lowest empty levels, i.e., the HOMO-LUMO gap, E_g^{HL}. Conversely in the limit of "small" n, LDA appears to reflect the correct quasi-particle gap; Table (2) gives the comparison between the HOMO-LUMO gap and the quasi-particle gap from LDA to experiment for small Si_nH_m molecule.

The size dependence of the quasi-particle and LDA HOMO-LUMO gaps and self -energy correlations are shown in figure 8.1[35]

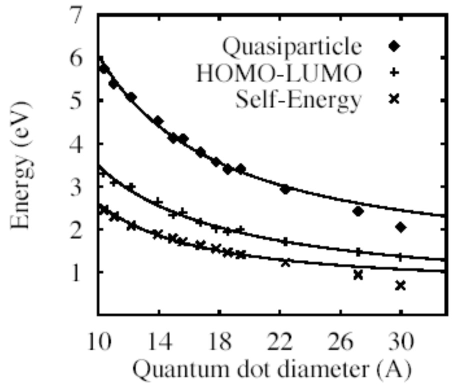

Figure 8.1Calculated quasi-particle (◊), HOMO-LUMO gaps (+) and self-energy Correlations (X) as a function of the quantum dot diameter d($\dot{A}$)

	ε_g^{HL}	ε_g^{qp}	GW
SiH_4	7.9	12.3	12.7
Si_2H_6	6.7	10.7	10.6
Si_5H_{12}	6.0	9.5	9.8
$Si_{14}H_{20}$	4.4	7.6	8.0

Table.2 HOMO-LUMO gaps and quasi-particle gaps E^{qp} calculated gaps E^{qp} for hydrogenated Si Clusters

Both gap values and self-energy correlations are enhanced substantially with respect to bulk values and are inversely proportional to the quantum dot diameter d as a result of quantum confinement [36]. The difference between the HOMO-LUMO gap and the quasi particles gap can be written as;

$$E_g^{qp} = E_g^{Hl} + \sum \quad \ldots\ldots\ldots \quad (41)$$

Where $\sum$ is the so-called self-energy correction. In the limit of $n \to \infty$, the self-correlation term vanishes and the HOMO-LUMO gap and quasi particle gap are equal.

8.2 Optical Gaps and Dielectric Screening

Since the quasi-particle gap refers to the energy to create a non-interacting electron-hole pair; one cannot compare these gaps directly to measurements of the optical gap. This issue is essentially important for quantum dots in which the exciton radius becomes comparable to the size of the dot [36]. In such circumstances, the Coulombic interactions are significantly larger than in the bulk. Moreover, the screening in small dots is not efficient which also results in an enhanced interaction. Using perturbation theory we write;

$$E_g^{opt} = E_g^{qp} - E_{coul} \ldots\ldots\ldots \quad (42)$$

Where E_g^{opt} is the optical gap and E_{coul} is the columbic interaction between electron and hole. Using *ab initio* pseudo-wavefunctions, the Coulombic interaction is written as:

$$E_{coul} = \int d\vec{r}_1 \left|\psi_e(\vec{r}_1)\right|^2 V_{scr}^h(\vec{r}_1)$$

$$= \int d\vec{r}_1 |\psi_e(\vec{r}_1)|^2 dr\, \varepsilon^{-1}(\vec{r}_1, \vec{r}) V^h_{unscr}(\vec{r})$$

$$= \iiint \varepsilon^{-1}(\vec{r}_1, \vec{r}) \frac{|\psi_e(\vec{r}_1)|^2 |\psi_h(\vec{r}_2)|^2}{|\vec{r}_1 - \vec{r}_2|} d\vec{r}\, d\vec{r}_1 d\vec{r}_2 \quad \text{..... (43)}$$

Where V^h_{scr} and V^h_{unscr} are screened and unscreened potentials due to the hole respectively and ψ_e and ψ_h are the electron- and hole- wavefunctions and ε^{-1} is the inverse of the microscopic dielectric matrix.

Formally, $\tilde{\varepsilon}^{-1}$ may be defined as:

$$\int \varepsilon^{-1}(\vec{r}_1, \vec{r}) \frac{1}{|\vec{r} - \vec{r}_2|} d\vec{r} \equiv \tilde{\varepsilon}^{-1}(r_1, r_2) \frac{1}{|\vec{r}_1 - \vec{r}_2|} \text{.....} \quad (44)$$

Then the exciton coulomb energy can be written as:

$$E_{coul} = \iint \tilde{\varepsilon}^{-1}(\vec{r}_1, \vec{r}_2) \frac{|\psi_e(\vec{r}_1)|^2 |\psi_h(\vec{r}_2)|^2}{|\vec{r}_1 - \vec{r}_2|} d\vec{r}_1 d\vec{r}_2 \quad \text{..... (45)}$$

An accurate calculation of E_{coul} requires the inverse dielectric matrix, for example when $\vec{r}_1$ and $\vec{r}_2$ in Eq. 42 are very close to each other, there will be practically no screening, and $\tilde{\varepsilon}^{-1} \approx 1$

To calculate the screening dielectric function $\varepsilon(\vec{r}_1, \vec{r}_2)$ of a particular quantum dot, one can first apply spatially modulated electric fields at several wave vectors to calculate the q-dependent polarizability (q) using a finite-field method.

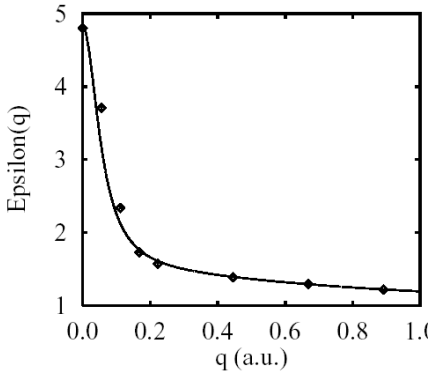

Figure 8.2 Dielectric functions for Si quantum dot.

The q-dependent dielectric function (q) is then obtained using a dielectric sphere model. The results for (q) of the $Si_{87}H_{76}$ quantum dots are shown in figure 8.2[36].

Figure 8.3 gives resulting optical gaps $E_g^{opt} = E_g^{qp} - E_{coul}$ along with the quasi-particle gaps and experimental results form Si: H nano crystals [35].

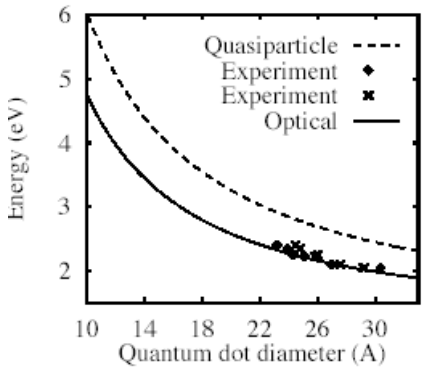

Figure 8.3 Calculated quasi-particle gaps (dotted lines), Optical gaps and experimental Absorption data from Si; H nc (x and ◊) as a function of the quantum dot diameter (A).

8.3 Optical Spectra

Recently developed linear response theory with in the time dependent density functional formalism provides a new mechanism for calculating excited states properties. This method known as the time dependent LDA (TDLDA) allows one to compute the true excitation energies form the conventional, time independent Kohn-Sham transition energies and wave functions [37].

Within the TDLDA, the electronic transitions energies are obtained form the solution of the following eigenvalue problem;

$$\left[\omega_{ij\sigma}^2 \delta_{ik}\delta_{jl}\delta_{\sigma T} + 2\sqrt{f_{ij\sigma}\omega_{ij\sigma}}\, k_{ij\sigma,kl\tau}\sqrt{f_{kl\tau}\omega_{kl\tau}}\right]\vec{F}_n = \Omega_n^2 \vec{F}_n \quad \ldots\ldots\ldots\ldots\ldots\ldots\ldots\ldots \quad (46)$$

Where $\omega_{ij\sigma} = \varepsilon_{j\sigma} - \varepsilon_{i\sigma}$ are the Kohn-Sham transition energies, $f_{ij\sigma} = n_{i\sigma} - n_{j\sigma}$ are the difference between the occupation numbers of the i-th and the j-the states, the eigenvectors $\vec{F}_n$ are related to the transition oscillator strengths and $k_{ij\sigma,kl\tau}$ is coupling matrix given by

$$k_{ij\sigma,kl\sigma} = \iint \phi_{i\sigma}^*(\vec{r})\phi_{j\sigma}(\vec{r})\left(\frac{1}{|\vec{r}-\vec{r}'|} + \frac{\partial v_\sigma^{xc}(\vec{r})}{\partial \rho_T(\vec{r}')}\right)\phi_{k\tau}(\vec{r}')\phi_{l\tau}^*(\vec{r}')d\vec{r}d\vec{r}' \quad \ldots\ldots\ldots\ldots\ldots \quad (47)$$

Where i, j, σ are the occupied states, unoccupied states and spin indices respectively, $\phi(\vec{r})$ are the kohn-sham wavefunctions and v_{xc} the LDA exchange-correlation potential [37].

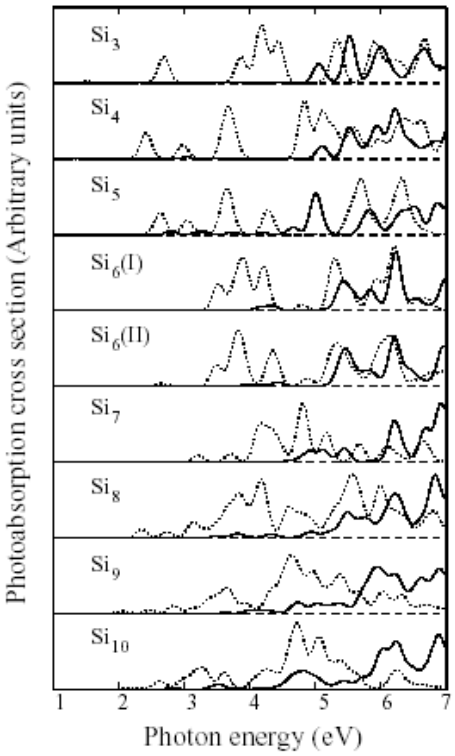

Figure 8.4 TDLDA absorption spectra of Si_n clusters (solid lines).
The dotted lines represent Kohn-Sham eigenvalues

In summary, real space calculations of quasi-particles and LDA band gaps, self–energy correlations, exciton coulomb energies, and optical gaps for silicon quantum dots are made using the finite pseudo-potential method. The results show enhanced self–energy correlations compared to the bulk and substantial exciton Coulomb energies due to quantum confinement. Moreover, in the limit of large systems, quasi-particle gap approaches HOMO-LUMO gap.

Such studies are expected to help explain the large difference between absorption and luminescence energies and the possible roles played by quantum confinement, surface states and relaxations associated with stoke's shift, towards a better microscopic understanding of visible luminescence from silicon nanocrystals and porous silicon.

Silicon is the leading semiconductor in microelectronic applications, and is thus the material of choice for reliable and low-cost opto electronic integrated circuits.

Today, however, bulk silicon is unsuitable as a light emitting material. Light can be emitted when electron recombines with the hole in the semiconductor .For this to happen effectively, the electron and hole must be close to each other and have overlapping

momentum distributions. Unfortunately, this overlap is not possible in macroscopic silicon crystals and hence has very low quantum efficiency. This limits its use in optoelectronics.

The direct application of nanostructures over the bulk is in photonics and electronics and potentially in extremely fast opto-electronic chip in which both electronic and optical functions are integrated in the same chip.

UNIT-NINE

9. Applications and Future Outlook

9.1 Applications

The tremendous range of both micro and macroscopic properties manifested by the size tuning of semiconductor nano crystals has provided them with the potential for use in a very broad application set [2]. This includes:

The potential value of quantum confined particles for non-linear optical and electro optical applications become of paramount importance in optical limiters, for eye protection and switching applications.

The tunability of the energy gap can be used to make light sources and detectors for specific use. In addition when discrete energy levels are formed with decreasing particle size, third order optical non-linearity are observed, which can be used in optical switches, wave guides, shutters and information processors.

Further use of nano particles has been demonstrated for metal insulator semiconductor field effect transistors (MISFET), photo detector, quantum dot lasers, solar cells, single electron transistors, infrared detectors, and optical memory devices.

Semiconductor nano particles are used as probes in biological diagnostics. In recent years a number of bottom-up technologies have been developed for producing isolated Si-nc (2-25nm) diameter that show significant potential for integration in to memory devices.

The large refractive index of silicon rich layer allows their use as core material in optical wave-guides.

The luminescence obtained from a Si-nc is shifted to a technologically useful range ~1.54 μm. This particular wavelength is of great technological importance due to the fact that the fiber optics cable employed in optical data transmission exhibits a transmission maximum at 1.54 μm. Additionally, erbium doped glass fiber is used as an amplifier for the optical data transmission.

Nano biotechnology and silicon chips become the basis of new diagnostics, analytical and drug delivery technique.

An example of a revolutionary diagnostic technology is a lab-on-a-chip device. This technology employs the possibility to have a personal diagnosis with in a few minutes using

a hand-held monitor around the size of a mobile phone instead of sending a sample of blood to a laboratory to be analyzed.

Smart pills- many forms of pharmacological treatment are best used in intense bursts delivered at predefined interval rather than as a continuous controlled dose. Nano porous silicon exhibits biocompatibility and bio degradability. Currently simple nano-fabricated devices are being developed consisting of reservoirs of drug capped with different thickness of diffusion membrane or soluble barrier. In the medium term micro electronically controlled devices open the caps.

Quantum dots are invisible until 'lit up' by UV light and can be made to exhibit arrange of colors depending on their composition [38]. This throws up opportunities in health applications for tracing the course of the rapevtic drugs or establishing circulatory problems in the human body.

The sponge structure of porous silicon is the cause of the high surface-volume ratio, which is typically of the order of $500m^2/cm^3$. The high reactivity of porous silicon layers in contact with chemical species is an advantage of p-Si as a sensing material. The sensing activity of p-Si ranges from NO_2, to humidity and to organic molecules.

P-Si micro cavities have been used as biosensor because of their response to DNA molecules and lipids, which allows distinguishing viral genetic chains and gram-negative bacteria.

Porous Silicon for Gas Sensor Application

Sensors are devices that produce a measurable change in out put to a known stimulus. Sensors are transducers, in that the incoming property to be measured is changed or transduced by the sensor into an electrical or other convenient output for the user [39].

Investigations and commercial interest of porous silicon materials are very intense in the recent years, due its potential applications in various areas such as gas and humidity sensors, photodiodes, optoelectronics, ultrasonic, surface sciences, astrophysics, biomedical sciences and in micro machining as a sacrificial layer in the formation of mechanical sensors like pressure sensors and accelerometers [40].

Investigations and commercial interest of porous silicon materials are very intense in the recent years, due its potential applications in various areas such as gas and humidity sensors, photodiodes, optoelectronics, ultrasonic, surface sciences, astrophysics, biomedical sciences

and in micro machining as a sacrificial layer in the formation of mechanical sensors like pressure sensors and accelerometers [40]. Tin-oxide-based p-Si gas sensors are widely used to detect inflammable and toxic gases. These sensors generally present a high sensibility and the detection of low levels of pollutants. The large surface to volume ratio of p-Si gives it the capability to react with gases and sense them readily.

The gas-induced modifications of p-Si properties (electrical and optical) are the sensing parameters of these devices.

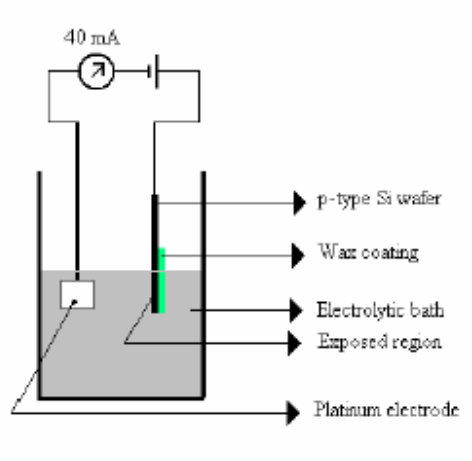

Figure.9.1 Anodization Experimental Setup

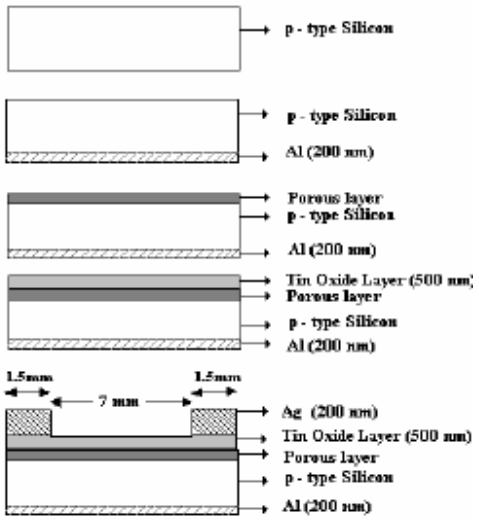

Figure 9.2 Fabrication stages of SnO2/PS Gas sensors

Memory Devices-Room Temperature Single Electron Memory Devices

i) The single electron shut off (SESO) memory is based on a new finding that the silicon band gap is effectively enlarged in very thin film by the quantum confinement effect. In this artificial wide-band gap silicon, the leakage current is suppressed, because the origin of the leakage is the transfer of an electron from the valence band to the conduction band, which is exponentially decreased as it is widened. This memory, which does not require capacitor to store charge, has simpler fabrication process than conventional DRAM, and better scalability toward higher density.

ii) MEID: - There is no doubt that the importance of non-volatile memories by which information is stored with out a battery, will be increased in mobile era. The problem of assuring non-volatility for all bits from the viewpoint of manufacturing and yield could be

solved by the newly proposed MEID memories. MEID memory enhances the manufacturing capability of non-volatile memories by using nano structures.

MEID stands for manufacturing enhancement by isolated-dots storage. The idea is simply to replace the floating gate of non-volatile memories by many dots (typically more than 100). In this way the charge is stored in those isolated dots, which results in superior robustness. MEID memory has demonstrated the non-volatile operation (beyond 10 years) even after 105 cycles write and erases [41].

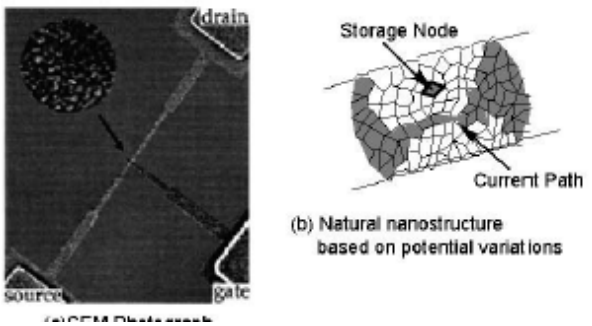

Figure 9.3The first room temperature single electron memory

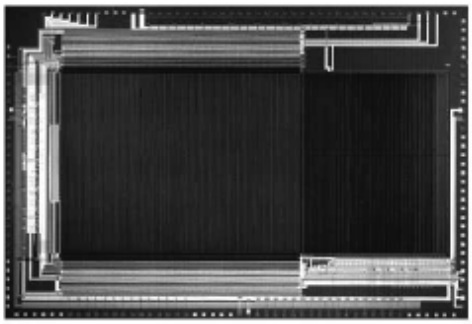

Figure 9.4 128-Mb single electron memory

Rapid Detection of Explosives –Nanowires; **Ultra –Sensitive Detectors**

UCSD researchers have developed a simple, fast, and inexpensive sensor to detect trace amounts of explosives. A silicon polymer has been made into a "nanowire" 2000 times thinner than a human hair, that detects compounds such as picric acid, nitrobenzene (NB), dinitrotluene (DNT) and trinitortluene (TNT) in air or seawater or on surfaces [42].

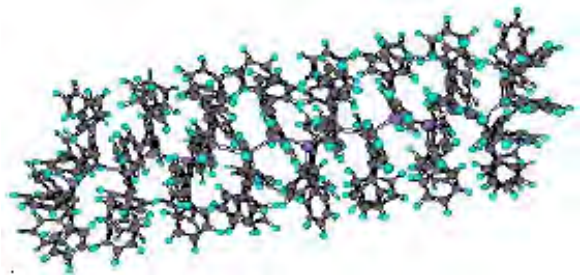

Figure 9.5 Nanowires designed for explosive detectors

Nanoporous Silicon Bioreactor

Researchers have developed a silicon-based bioreactor. Initial studies have been done with primary hepatocytes from rat, stabilized in cell-sized pores of porous silicon. Physiological and biochemical activities of the cells were quantitatively evaluated over time. The hepatocytes adhered to the silicon and maintained viability similar to controls.

Silicon based cells also maintained liver specific functions, including urea synthesis and albumin secretion [42]. This invention has applications for further development in many areas, from tissue engineering to drug discovery applications.

Smart Dust –A New Porous Silicon Based Technology

A new nanotechnology ("smart Dust") with state-of-the-art applications in almost every field of use, ranging from biological sensing and screening to communications technology. The invention utilizes micron-sized particles of silicon that have been etched and then chemically modified in such a way that each individual particle has its own addressable identity [42]. This feature allows one to use thousands of the particles together, each with its own "tag", for high sensitivity chemical or biological sensing diagnostics, and low and high-through put screening of bimolecular compounds.

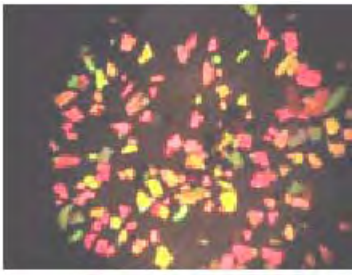

Figure 9.6. Smart Dust

Magnetic Porous Silicon Photonic Crystals

Porous silicon (P-Si) is a particularly attractive material for biological and high technology applications because of the ease with which the optical properties; pore size and surface chemistry can be manipulated. The position, width and intensity of spectral reflectivity peaks are controlled by current density, waveform and solution composition used in the electrochemical etch. This allows the preparation of p-Si photonic crystals that can display any number of colors with in the visible spectrum with high color saturation and resolution, highly desirable features for information display. Researchers at the University of California, San Diego, have converted these films in to micron-sized particles (so-called "smart Dust").

Amphiphilic Magnetic Porous Silicon Photonic Crystals

Recently, magnetically switch able micro-sized photonic crystals that can be induced to flip between a colored photonic crystal face and a black, non-reflective surface in an

oscillating magnetic field could be demonstrated [42]. This property makes this an excellent material for use in display applications. In addition, magnetic Smart Dust has now been constructed with amphiphilic properties. This allows the micron-size crystals to self-align at the interface between immiscible liquids and effectively encapsulates suspended droplets.

9.2 Future Outlook

Understanding how size and surface effects change optical and electronic property of nano structures is a key step in nanoscinece. Experimentalists and quantum simulation experts are working together to establish a basic knowledge of the structured and optical properties of semiconductor nanostructures. Some day a scientist will know exactly how to produce a nano widget to detect a deadly pathogen. Perhaps the widget must emit blue light, and the scientist will know that using a nano particle of a given size and density produces the desired wavelength.

Next dream is to make truck films on which germanium particles are closer together and touching, which is how they will be in real-world applications. Unfortunately, when they touch, nano semiconductor particles tend to lose some of their special electronic properties. In fact, surface passivation technique keeps the particles isolated.

Silicon based chips are expected to remain the mainstream technology for logic and memory applications for as far into the future as can be reliably foreseen.

The continued performance improvement of modern silicon computer chips has largely been driven by a reduction in the minimum feature size of the individual transistors fabricated on silicon wafer. Reduction in size not only allows more transistors to be fabricated on a given piece of silicon, but also allows for faster operation of these transistor and lower driving voltage. According to the international technology road map for semiconductors (ITRS), this minimum feature size is projected to reach 10nm in 2018; its current value is 53nm [43].

Nanotechnology is the future hope in the life science. One such prediction is nanorobot therapeuties. In the future, it has been envisaged that nanorobots will float around the body and carry out targeted healing jobs. They may take many years to come to flourish and may spin a whole new range of unrelated technologies along the way.

For the next couple of decades, the introduction of new silicon based concepts to accomplish further size reduction is much more likely than a replacement by completely new technologies such as molecular or carbon nanotube devices or single electron transistors. However, new silicon-based materials containing nanostructures will be needed to achieve this goal and also to keep pace with Moore's law, predicting that the numbers of transistors on an integrated circuit will double every 18 months.

Nanotechnology is expected to have an impact on nearly every industry. The research community is actively perusing hundreds of applications in nanomaterials, nano electronics and bionanotechnology. Nanodevices and nanoelectronics will have applications in medical treatments and diagnostics, faster, computers and in sensors.

Silicon-based nanostructures with special emphasis on light emission have been the subject of a recent review. An example is doping of a bulk material with a suitable impurity such as erbium. Erbium atoms in their Er^{3+} ionic states are responsible for the emission of photons $1.54\,\mu m$. This emission, which results from an extra–4f shell transition, is used to amplify light in Er-doped optical fibers for optical communications and is actively investigated in silicon [23]. Current understanding of the light emission in Er-Si suggests two possible excitation processes: a) excitation by a photon from an e-h recombination, with in the Si gap, at an Er-related energy level and b) hot carrier impact ionization .To relax the energy two mechanisms have been proposed:

i) back transfer of energy from an Er^{3+} level to states in the energy gap of Si; and

ii) transfer of energy from the Er^{3+} ion to free electrons in silicon via an Auger process.

Two issues have to be considered: the excitation light emission process is slow (ms), which presents a barrier for high frequency operation and the emission intensity quenches rapidly with increasing temperature from cryogenic levels to 300K.

Doping Si-SiGe hetero-structures with Er and Er/O is a development under investigation in order to take advantage of band gap engineering offered by Si/SiGe hetero-junctions.

Although progress in integrable Si-based detectors and wave guides is very encouraging, electro luminescent devices have still some way to go to meet the requirement of quantum efficiency, high operating frequency and life time necessary to compete with the hybrid solution using III-V optoelectronic systems. Moreover, issues like compatibility with the processing steps of a Silicon CMOS plat form pose enormous challenges to potential

solutions involving hydrogen incorporation since this would limit processing temperatures to about 400^0c.

Conclusion

The science of miniaturizing and the subsequent technology has brought a new drastic change in materials properties. Quantum confinement effects, by large, attributed to these changes. It could be seen that the widening of the energy gap at nanoscale is due to this effect.

Quantum size effects bring the discritization of the density of states and the excitonic radiative recombination is responsible for the resulting photoluminescence. Such optical properties are due to the excitonic radiative recombination.

In addition to the quantum confinement effects, other mechanisms such as surface states play a role for the visible photoluminescence of silicon nanocrystals.

Porous silicon materials have got strong photoluminescence efficiency at room temperature unlike bulk silicon, which has low PL efficiency due to its indirect energy band dap. Both experimental and theoretical studies conducted recently seem to indicate that short–range crystallinity, passivation and confinement combine to produce p-Si photoluminescence.

The introduction of rare earth dopants like Er in silicon nanocrystals in silicon dioxide layers is presently a major activity. The nanocrystals and rare earth ions interact, leading to a strongly enhanced photoluminescence from the rare earth ions.

AFM analysis of silicon nanostructures synthesized in different techniques show that silicon at nano scale has crystalline structure and nearly spherical geometry .The synthesis methods are mostly conducted under vacuum condition due to the reactive nature of silicon clusters.

Structures of silicon nanocrystals could also be computed applying simulated annealing for lower structures. Because the number of possible configurations grows exponentially with the number of atoms, there are no computationally tractable techniques for determining the ground state for a cluster of more than a few dozens of atoms.

Within the local density approximation, in the limit of very large system ($n \to \infty$) the quasi particle gap approaches HUMO-LOMO gap. Conversely, in the limit of small n LDA appears to reflect the correct quasi particle gap. The time dependent LDA enables to compute the true excitation energies from the conventional time independent transition energies and wavefunctions.

The spectacular features that silicon nanocrystals and porous silicon exhibit made them essential components in semiconductor technology. The applications in nanoelectronics (powerful computers, small mobile phones etc.), nanobiotechnology, nanomedicine and environmental monitoring are front line potentials of these materials.

Despite the progress in nanoscience and nanotechnology, there are big challenges that influence whether nanotechnologies will be used routinely with industrial process.

The difficulty in scaling a process up from laboratory to an industrial operation, lack of understanding of nanoscale properties and the techniques to characterize and engineer them to form useful materials and products, insufficient knowledge to synthesize complex heterogeneous nano-structured, large scale, self assembled nanolayers are some of the barriers in the area.

It is then tremendously important for those working in the field of semiconductor nanocrystals to understand the complexities and contrasts and come out with better performance nanostructures that derive towards a better device technology and civilization.

In fact it would be a long-term vision for peoples in developing countries such as ours to take part in the utilization of functional devices that could be achieved from this newly flourishing technology.

References

[1] http://www.chem.wisc.edu

[2] http://www.meliorum.com/

[3] http://www.llnl.gov/str/

[4] http://search.msn.com/

[5] http://www.swissre.com/

[6] Introduction to nanotechnology, P. Poole, Jr. and J. Owens.

[7] Nanoscience and nanotechnologies, The Royal society and the Royal academy of engineering, 1 July 2004.

[8] http://www.ct.infn.it/matis

[9] Quantum dots: phenomenology, photonic and electronic properties Modeling and technology, Frederic Boxberg and Jukka and Tulkki.

[10] Dielectric suppression of nanosolid silicon, Nanotechnology, 15(2004) 1802-1806.

[11] Handbook of Thin films Materials, H.S.Nalwa, volume 5: Nanomaterials, and Magnetic Thin films.

[12] Role of Hydrogen on the HOMO-LUMO states of light emitting silicon quantum dots: an empirical Pseudo-potential calculation, S.K.Ghoshal, Asian Journal of Spectroscopy, 7(2003) 49-68.

[13] Fluorescent semi conducting nanocrystals show their luminescence, CLEFS CEA. No.52- summar2005.

[14] Url: http:||sience.unitn.it/~semicon/

[15] http://www.webelements.com

[16] http://www.webelements.com

[17] Nanocrystals: “Keeping pace with Moor’s law,” Arne Nylandsted and BrianBech Nielson.

[18] The Optical properties of silicon nanocrystals and the role of hydrogen pasivation, A.R.Wilkinson

[19] http://en.wikiapedia.org/wiki/porous

[20] Porous silicon: Silicon quantum dots for photonic applications, L.Pavesi and R.Guardini, Brazilian Journal of physics, Vo l, and 26, no.1 March 1996.

[21] Porous silicon, Z.Gaburro, N.Daldosso and L.Pavesi.

[22] http;//www.azom.com/

[23] Silicon based optoelectronics: Progress and challenges, Tamin P.SIDIKI, CIVIA M. Sotomayor, Tr.J.of physics, 23 (1999).

[24] http://nano.ee.uec.ac.jp

[25] Chemistry of nanoscale semiconductor clusters, Jun Pan, Atul Bahel and Mushti V. Ramakrishna, arXiv: chem.-phy/9506002vl3 June 1995.

[26] Size controlled highly luminescent silicon nanocrystals: A SiO/SiO_2 supper Lattice Approach, M. Zachrias, J. Heitman, R. Scholaz U. Kahler, and M. Schemidt and J.Blaisng.

[27] Silicon Nanostructures For photonics, L.Pavesi, P.Bettoti, M.Cazzanelli, S.Cella, N.Daldosso L.Dal Negro, B.Danese, Z.Gaburro.

[28] Optical and electronic correlation effects in silicon quantum dots, S.K.Ghoshal, K. P. Jain and R. J. Elliott.

[29] Optical properties of nano silicon, STRIPATHY, R.K.SONI, S.K.Ghoshal and K.P.JAIN, Bull.Mater.Sci, vol.24, No.3, June 2001, pp.285-289.

[30] Changes in the electronic properties of silicon nanocrystals as a function of Particle size, T.VanBurren, L.N.Dinh, L.L.chase, W.J.Seikhaus, and L. J.Terminello, Physical review letter, vol 80, no.17, 27 April 1998.

[31] Electrical properties of silicon nanocrystals embedded in an ultra thin oxide, Nanothecnology 10 (1999) 127-131.

[32] http://www.ece.rochester.edu.

[33] http://jrc.cem.umn.edu.

[34] Using silicon to understand silicon: Doping of Nanostructures, James R. Chlikowsky, The electronic society interface, spring 2005.

[35] http://jrc.cems.umn.edu/

[36] Optical Gaps and Screening in Quantum dots, James R. Chlikowsky and Serder Ogut.

[37] Optical excitations in Nanostructures: Application of Time Dependent Density Functional Theory to Sin (n= 3-10), Igor Vasiliev, Serder Ogut, and R. Chelikowsky.

[38] http://www.nano.org.uk

[39] http://www.worldcatlibraries org/

[40] Investigations on Nanoporous silicon for gas sensor applications, N. Sankara, R.Sriram and B. Santhi.

[41] Room temperature single electron Devices, YANO Kazuo.

[42] http://invent.ucsd.edu

[43] The development of nanocrystalline silicon for engineering microelectronics and Nanocrystalline applications, Christopher C.Striemer, Reshikesh Krishnan and Philippe M. Fauchet, JOM.Oct.2004.